AGU PUBLICATIONS

JGR

Journal of Geophysical Research: Space Physics

RESEARCH ARTICLE
10.1002/2015JA021298

Key Points:
- Bending arcs are polar arcs that split from the prenoon or postnoon oval and bend into the polar cap
- Bending arcs form during dayside reconnection
- The initial location of regular polar arcs is determined by IMF B_y conditions at least 1–2 h earlier

Correspondence to:
A. Kullen,
kullen@kth.se

Citation:
Kullen, A., R. C. Fear, S. E. Milan, J. A. Carter, and T. Karlsson (2015), The statistical difference between bending arcs and regular polar arcs, *J. Geophys. Res. Space Physics*, *120*, 10,443–10,465, doi:10.1002/2015JA021298.

Received 2 APR 2015
Accepted 17 NOV 2015
Accepted article online 19 NOV 2015
Published online 18 DEC 2015

The statistical difference between bending arcs and regular polar arcs

A. Kullen[1], R. C. Fear[2], S. E. Milan[3], J. A. Carter[3], and T. Karlsson[1]

[1]Space and Plasma Physics, School of Electrical Engineering, KTH Royal Institute of Technology, Stockholm, Sweden, [2]Department of Physics and Astronomy, University of Southampton, Southampton, UK, [3]Department of Physics and Astronomy, University of Leicester, Leicester, UK

Abstract In this work, the Polar UVI data set by Kullen et al. (2002) of 74 polar arcs is reinvestigated, focusing on bending arcs. Bending arcs are typically faint and form (depending on interplanetary magnetic field (IMF) B_y direction) on the dawnside or duskside oval with the tip of the arc splitting off the dayside oval. The tip subsequently moves into the polar cap in the antisunward direction, while the arc's nightside end remains attached to the oval, eventually becoming hook-shaped. Our investigation shows that bending arcs appear on the opposite oval side from and farther sunward than most regular polar arcs. They form during B_y-dominated IMF conditions: typically, the IMF clock angle increases from 60 to 90° about 20 min before the arc forms. Antisunward plasma flows from the oval into the polar cap just poleward of bending arcs are seen in Super Dual Auroral Radar Network data, indicating dayside reconnection. For regular polar arcs, recently reported characteristics are confirmed in contrast to bending arcs. This includes plasma flows along the nightside oval that originate close to the initial arc location and a significant delay in the correlation between IMF B_y and initial arc location. In our data set, the highest correlations are found with IMF B_y appearing at least 1–2 h before arc formation. In summary, bending arcs are distinctly different from regular arcs and cannot be explained by existing polar arc models. Instead, these results are consistent with the formation mechanism described in Carter et al. (2015), suggesting that bending arcs are caused by dayside reconnection.

1. Introduction

Auroral arcs appearing poleward of the main oval are often grouped into small-scale Sun-aligned arcs that have a rather high occurrence frequency [e.g., *Valladares et al.,* 1994, and references therein] and large-scale polar arcs, which appear during about 10–16% of the time [*Kullen et al.,* 2002]. On global imagers with a spatial resolution of about 30–50 km such as the UV camera on the Polar satellite, only the large-scale polar arcs can be observed. The present study is based on a list of polar arcs that have been identified with Polar UV images [*Kullen et al.,* 2002]; thus, the focus is on large-scale polar arcs. As these often extend from the nightside to the dayside oval, they are sometimes referred to as theta aurora [*Frank et al.,* 1982] or more commonly as transpolar arcs. Here we refer to all large-scale polar arcs as "polar arcs" rather than transpolar arcs, as some of the arcs studied in this work are (at least during part of their lifetime) not connected to the dayside oval. Due to the diversity of polar arc formation and evolution, *Kullen et al.* [2002] sorted all polar arcs of their large statistical study into five groups (expanding on a classification by *Gussenhoven* [1982]): oval-aligned arcs, moving arcs, nightside originating arcs (in their paper, *Kullen et al.* [2002] referred to these as "midnight arcs"), multiple arc events, and bending arcs. In the present study, we refer to these categories using the same definitions as in *Kullen et al.* [2002].

1.1. Polar Arc Observations: Dependence on Solar Wind Conditions and Evolution

The dependence of polar arc occurrence and motion on interplanetary magnetic field (IMF) has been known for a long time (see, e.g., the excellent review by *Zhu et al.* [1997] or *Kullen* [2012], and references therein). Many observational studies confirmed that polar arcs are a predominantly northward IMF phenomenon [e.g., *Gussenhoven*, 1982; *Ismail and Meng*, 1982; *Frank et al.,* 1986; *Kullen et al.,* 2002]. The initial location of polar arcs depends on the IMF B_y sign [e.g., *Gussenhoven*, 1982; *Elphinstone et al.,* 1990; *Kullen et al.,* 2002] and magnitude [*Fear and Milan*, 2012a]. Most northern hemisphere polar arcs form close to the dusk oval side during duskward IMF and close to the dawn oval side during dawnward IMF. Not only the initial location but also the dawn-dusk motion of polar arcs is controlled by IMF B_y [*Craven et al.,* 1991; *Kullen et al.,* 2002; *Fear and Milan*, 2012a].

In those cases with rather constant IMF conditions the hours before and after arc formation, polar arcs do not show any considerable poleward motion during their lifetime [*Kullen et al.,* 2002; *Fear and Milan*, 2012a]. Such arcs are often referred to as oval-aligned arcs [*Murphree and Cogger*, 1981; *Elphinstone et al.,* 1990; *Kullen et al.,* 2002].

Some arcs that form at the dawn or dusk side of the oval, move toward the noon-midnight meridian, some even over the entire polar cap. Such events were classified by *Kullen et al.* [2002] as "moving arcs", although they are oval-aligned at the time of formation. *Cumnock et al.* [1997] discovered that those moving arcs forming on the dawnside and propagating subsequently over the polar cap toward the dusk oval side appear typically in connection with an IMF B_y sign change from dawnward to duskward. For polar arcs moving in the opposite direction, an IMF B_y sign change from dusk- to dawnward is observed. During IMF conditions with only one clear IMF B_y sign change during constantly northward IMF, nearly always a polar arc forms that moves across the polar cap [*Cumnock*, 2005]. Polar arcs are absent during such conditions only if the solar wind energy flux ($\sim vB^2$) is extremely low, probably due to the correlation between polar arc luminosity and solar wind energy flux [*Kullen et al.,* 2008].

A change in sign of IMF B_y is, however, not required for a polar arc to move toward the noon-midnight meridian; a significant increase or decrease of the B_y component is sufficient. *Kullen et al.* [2002] reported such a case where the arc did not cross the noon-midnight meridian. This fits well with *Cumnock*'s [2005] observation that most polar arcs appearing in connection with a B_y sign change had already separated from the oval as $|B_y|$ decreased with respect to B_z, reached the noon-midnight meridian after the B_y sign change has taken place, and continued their motion toward the other oval side as $|B_y|$ increases again with respect to B_z. This indicates that an IMF B_y sign change or $|B_y|$ decrease does not cause the formation of the arc itself but the poleward motion of an existing oval-aligned arc, as argued by *Milan et al.* [2005].

Contrary to *Cumnock*'s [2005] observations, most moving arcs reported by *Kullen et al.* [2002] started to form 10–60 min after an IMF B_y sign change took place, rather than before the sign change. If the scenario described above is generally valid, this would mean that the time it takes until the nightside auroral precipitation pattern is affected by new IMF conditions must exceed 10–60 min. *Milan et al.* [2005] suggested that the time scale on which the IMF B_y component affects the motion should be much shorter than the time scale on which it affects the location at which the arcs form. They assume that the motion of an existing polar arc is driven by convection in the polar cap stirred by high-latitude lobe reconnection during northward IMF. Thus, the arc motion should be determined by the current IMF conditions. The statistical results by *Fear and Milan* [2012a] revealed a long time delay between IMF B_y conditions and its effect on the initial location of polar arcs. In their analysis, the correlation peaked if the IMF was lagged by ~3–4 h.

Several observational reports show that not all polar arcs separate from the dawnside or duskside oval and move poleward. There exist also polar arcs that evolve from the nightside oval and expand sunward into the polar cap instead of separating from the dawn or dusk oval [*Craven et al.,* 1986; *McEwen and Zhang*, 2000; *Kullen et al.,* 2002; *Goudarzi et al.,* 2008; *Fear and Milan*, 2012b]. Here we refer to these as nightside originating arcs, although *Kullen et al.* [2002] used the term midnight arcs. Furthermore, a few cases have been reported where several arcs appear simultaneously in the polar cap, which may emerge from both oval sides and the nightside oval [*Newell et al.,* 1999; *Kullen et al.,* 2002]. These are referred to as multiple arcs.

In *Kullen et al.* [2002] a special type of polar arc has been observed that that has not previously been reported. These so-called bending arcs are often extremely faint, and thus difficult to detect on global imagers. They typically exist only for some tens of minutes, which is much shorter than the average polar arc lifetime (e.g., *Kullen et al.* [2002] reported an average polar arc lifetime of 2 h). Bending arcs form such that the dayside part of the arc moves poleward, while the nightside end does not show a considerable motion such that this auroral feature resembles a hook-shaped arc sometime after its formation. Note that *Kullen et al.*'s [2002] bending arcs should not be confused with so-called hook-shaped transpolar arcs that have been reported occasionally [e.g., *Meng and Akasofu*, 1976; *Ismail and Meng*, 1982; *Gusev and Troshichev*, 1986], or the bending arc reported by *Fear and Milan* [2012b]. None of those reported cases show the characteristic development of the bending arcs identified in *Kullen et al.* [2002] and are thus most probably not the same auroral feature. The events described in *Meng and Akasofu* [1976] and *Ismail and Meng* [1982] are most probably true transpolar arcs which during part of their lifetime become strongly bent, similar to the moving

arc example shown in *Kullen et al.* [2002] (their Figure 5, moving arc at 23:40 UT). *Fear and Milan*'s [2012b] bending arc, on the other hand, resembles *Kullen et al.*'s [2002] nightside originating arcs (their Figure 5, midnight arc example). *Gusev and Troshichev* [1986] reported small-scale Sun-aligned polar arcs in the dayside polar cap; some of which are strongly bent.

As reported in *Kullen et al.* [2002], most bending arcs appear in connection with an IMF B_z sign change. The possibility of an IMF B_z sign reversal from northward to southward as trigger for the formation of regular polar arcs has been discussed before in terms of a merging line jump from high to low latitudes [*Newell and Meng*, 1995; *Newell et al.,* 1997; *Chang et al.,* 1998]. However, aside from the case of bending arcs, *Kullen et al.* [2002] found no systematic correlation between IMF B_z sign change and polar arcs. As reported by *Kullen et al.* [2002], bending arcs show a distinctively different dependence also on other solar wind parameters: contrary to other polar arcs they appear during near-zero IMF B_z conditions and low values of the solar wind energy flux. Also, the IMF B_y and B_x dependence deviates from what is found for other polar arc types. A majority of northern hemisphere polar arcs appear during negative IMF B_x (southern hemisphere arcs during positive IMF B_x [*Elphinstone et al.,* 1990]). Northern hemisphere bending arcs occur much less often during negative IMF B_x than regular polar arcs. Furthermore, bending arcs appear, in opposite to most polar arcs, on the dawn oval side during duskward and dusk oval side during dawnward IMF.

1.2. Models for Regular Polar Arcs

Due to similar particle characteristics of polar arcs and discrete arcs within the main oval it has often been assumed that transpolar arcs appear on closed field lines that origin in the plasma sheet or its boundary layer [e.g., *Peterson and Shelley*, 1984; *Frank et al.,* 1986]. It was first suggested by *Frank et al.* [1986] that the plasma sheet would be bifurcated, where the bifurcated tongue maps high into the lobes and to a theta aurora in the middle of the polar cap. Observation of filamentary plasma sheet extensions into the lobes during a transpolar arc event [*Huang et al.,* 1989] and recent observations of closed field lines filled with atypically hot plasma within the lobes [*Fear et al.,* 2014] during a transpolar arc event shows that such a plasma sheet topology may exist.

To trace the source region of transpolar arcs, it is necessary to consider the topology of the magnetotail during nonzero IMF B_y conditions. *Fairfield* [1979] reported the presence of a magnetotail B_y component, which is proportional to that observed in the IMF. This was explained theoretically by *Cowley* [1981] as the consequence of dayside reconnection in the presence of nonzero IMF B_y. He also predicted that this would lead to a rotation of the tail plasma sheet around the x axis, which increases tailward. Both a neutral sheet twist [*Kaymaz et al.,* 1994] and a plasma sheet twist, which increases with distance downtail [*Tsyganenko et al.,* 1998], were later-on confirmed on a statistical basis. *Owen et al.* [1995] observed that during northward IMF conditions the IMF B_y-induced plasma sheet twist becomes much stronger than during southward IMF, which was later-on confirmed statistically by *Tsyganenko and Fairfield* [2004]. In MHD simulations by *Kullen and Janhunen* [2004], strongest plasma sheet twists occur for $B_z \geq |B_y|$, where high-latitude lobe reconnection dominates. During lobe reconnection, open magnetic field lines originating in the northern hemisphere are connected to solar wind field lines south of the magnetosphere. When the solar wind drags these field lines in an antisunward direction, these overdraped open field lines exert for nonzero IMF B_y a strong torque on the magnetotail, which is probably the reason for a much stronger tail twist than during southward IMF. MHD simulations also show that during IMF conditions with $B_z > |B_y|$, the plasma sheet thickens. As a result the far tail plasma sheet appears at highest northern latitudes along the dusk (dawn) flank for duskward (dawnward) IMF B_y and northward B_z.

Meng [1981] interpreted polar arcs occurring during nonzero IMF B_y as the poleward boundary of an expanded auroral oval. Three decades later *Newell et al.* [2009] suggested that this is in most cases the correct scenario, as many polar arcs that seem to be clearly separated from the oval on global images are in fact connected with the main oval by a continuous region of ion population when looking at Defense Meteorological Satellite Program (DMSP) data. Also, *Makita et al.* [1991] suggested that oval-aligned arcs may map to a strongly displaced plasma sheet boundary at highest latitudes. *Kullen and Janhunen*'s [2004] MHD simulations confirm that such a scenario would be possible. The open-closed field line boundary for IMF conditions with IMF $B_z > |B_y|$ is strongly polewardly displaced on the duskside for duskward (and dawnside for dawnward) IMF at which an oval-aligned arc may possibly occur.

For those arcs moving over the entire polar cap, a slightly different model has been proposed. *Kullen* [2000] showed how a reconfiguration of the tail may look like after a sign reversal of IMF B_y assuming that the tail plasma sheet will change successively its B_y-induced twist into the opposite direction. They showed by modifying the semiempirical *Tsyganenko* [1989] magnetosphere model that a magnetotail topology with opposite twist of near-Earth and far tail neutral sheet may result in a strip of closed field lines that extend high into the lobes and into the polar cap. The strip appears to "move" over the polar cap as the rotation front caused by the new IMF B_y direction moves tailward. Simulations of an IMF B_y sign change during northward IMF from several different MHD models have all produced similar results [e.g., *Slinker et al.,* 2001; *Kullen and Janhunen*, 2004; *Naehr and Toffoletto*, 2004]. They differ in details but in all simulations, the tail plasma sheet undergoes a major reconfiguration that starts in the near Earth tail flanks and propagates inward (toward the tail center) and tailward. All models reproduce a closed field line strip that moves from dawn to dusk (dusk to dawn) in the ionosphere, as would be expected for a moving polar arc that occurs after an IMF B_y sign change from dawn to dusk (dusk to dawn). These results suggest that tail changes are closely connected to changes in the ionospheric open-closed boundary (and implicitly the motion of a moving arc). Note, that in an MHD simulation, an IMF B_z sign reversal during southward IMF does not result in any bifurcation of the model polar cap boundary (unpublished results from the study by *Kullen and Janhunen* [2004]), probably because of the much smaller tail twist for nonzero IMF B_y during negative IMF B_z [*Kullen and Janhunen*, 2004; *Tsyganenko and Fairfield*, 2004].

Other polar arc models involve the concept of a return flow blockage in convection cells, which would lead to a pileup of closed flux that protrudes into the polar cap [*Tanaka et al.,* 2004; *Milan et al.,* 2005]. In both models it is assumed that polar arcs form on the nightside half of the oval and grow toward noon. *Tanaka et al.* [2004] simulated an IMF B_y sign change during northward IMF and analyzed the connected changes in plasma convection throughout the magnetosphere. Their simulation results indicate that the formation of a polar arc is caused by transient convection after a sign change of IMF B_y, where the growth of new lobes blocks the return path toward the dayside of those closed field lines that have been generated in the old merging cell. Losing their return path, these closed field lines accumulate on the nightside, causing both a plasma sheet kink and the formation of a polar arc along the nightside oval. While *Tanaka et al.*'s [2004] model addresses only to those polar arcs that occur in connection with an IMF B_y sign change (i.e., moving arcs), *Milan et al.* [2005] proposed a theoretical concept that would explain the formation of polar arcs during nonzero IMF B_y in general.

Milan et al.'s [2005] model differs from other models by suggesting that tail reconnection is required for the formation process of polar arcs. In that model it is assumed that the closure of lobe magnetic flux through magnetotail reconnection leads to a local pileup of closed flux into the lobes, resulting in a polar arc that forms at the nightside oval and expands toward noon. The model predicts that the polar arc forms at the location where dawnward and duskward convecting field lines separate, assuming that the initial location of the arc depends on the distortion of the magnetotail topology by IMF B_y penetration effects. It is known that due to the IMF B_y penetration process during nonzero IMF B_y, field lines close in a manner such that the northern and southern ionospheric foot points of the newly closed field lines are strongly displaced relative to each other in local time (i.e., azimuthally bent closed field lines). Consequently, the return flow of these field lines is asymmetric and results in fast azimuthal plasma flows along the nightside oval. These so-called "TRINNIs" (Tail Reconnection during IMF Northward Non-substorm Intervals) appear regularly during northward IMF with nonzero IMF B_y [see *Grocott et al.,* 2003, 2004, 2005, 2007] and are interpreted as the signatures of magnetotail reconnection. *Milan et al.* [2005] proposed that at the eastward or westward end of a TRINNI the forces on opposite halves of the field lines will be broadly equal and opposite; thus, a subset of the closed field lines will be unable to convect back to the dayside causing the formation of an arc that grows into the polar cap. Later on, *Fear and Milan* [2012b] confirmed with the help of Super Dual Auroral Radar Network (SuperDARN) data that most polar arcs form indeed at the eastward or westward end of a TRINNI.

The goals of this paper can be described in the following way: We want to clarify whether the results by *Fear and Milan* [2012a, 2012b] can be reproduced with an independent data set. This is done by using the polar arc list from *Kullen et al.* [2002], which is based on a different imager and covers a different time period. The question arises whether the results by *Fear and Milan* [2012a, 2012b], who only distinguished between static

and moving polar arcs, are applicable to each of the different polar arc types described in *Kullen et al.* [2002], especially bending arcs. The latter are not covered in the *Fear and Milan* [2012a, 2012b] data analysis due to more restrictive polar arc selection criteria regarding arc lifetime than in *Kullen et al.* [2002].

In this work we focus on the initial location of polar arcs. From the different observational results described above it is clear that polar arcs form at a location that depends on B_y a while beforehand. How long beforehand is reinvestigated here. In addition, we want to find out whether the occurrence of a polar arc at the eastward or westward end of a TRINNI can be confirmed for each of *Kullen et al.*'s [2002] polar arc type separately, which would indicate that all polar arc types may be connected magnetotail reconnection processes.

The results of *Kullen et al.* [2002] already suggest that bending arcs deviate in many aspects from other polar arc types. Thus, the main focus of the study is on these arcs. *Carter et al.* [2015] have recently presented a case study about one of *Kullen et al.*'s [2002] bending arcs, where it is suggested that it may have the same formation mechanism as poleward moving auroral forms (PMAFs). PMAFs are transient auroral features that split off the dayside oval and move within some minutes poleward before they disappear. They are generally believed to be the auroral signature of pulsed flux transfer events (FTEs) [e.g., *Fasel,* 1995; *Milan et al.,* 2000; *Sandholt and Farrugia*, 2007]. With the present study we want to statistically verify whether the formation mechanism suggested by *Carter et al.* [2015] may be applicable for bending arcs in general.

1.3. Instrumentation

The entire study is based on the polar arc data set of *Kullen et al.* [2002]. The events of that data set were identified by visual inspection of global auroral UV images from the Polar spacecraft, covering a 3 month time period in northern hemisphere winter 1998/1999. The UV imager on Polar had during 1998/1999 a near global view on the northern hemisphere about 75% of the time. The UV camera on Polar images the aurora every 37 s in the ultraviolet region of the spectrum using four narrow band filters, two of which measure in the Lyman-Birge-Hopfield band (LBH). The integration times of each image are 18 and 36 s, respectively. In *Kullen et al.* [2002] LBH long images with an integration time of 36 s were used to provide maximal brightness of the images and to avoid absorption effects (LBH long emissions of 160–180 nm are not significantly absorbed by the atmosphere). The resolution of the images is 0.5° in latitude at apogee; thus, a single pixel projected to 100 km altitude from apogee is approximately 50×50 km. Away from apogee the imager can detect even smaller spatial scales (35×35 km). The plots are shown in a polar view, and the magnetic apex coordinate system [*Richmond*, 1995] with corresponding magnetic local time (MLT) and latitude (corrected geomagnetic latitude (CGlat)) is used. For more details on the UV instrument on Polar, see *Torr et al.* [1995].

For the investigation of a possible correlation between polar arc location and IMF conditions, 1 min resolution solar wind data from the OMNI data set are used (available at omniweb.gsfc.nasa.gov). That data set consists of measurements from the nearest solar wind monitor at each given point of time. The propagation time to the Earth's bow shock is calculated accurately and already included in the data [*King and Papitashvili*, 2005]. By using 1 min resolution OMNI data instead of 5 min averaged ACE data (at 220 *Re* sunward from the Earth) with a simple estimate of the propagation time by using 24 h averaged solar wind speed values (as was done in *Kullen et al.* [2002]), the dependence of polar arc evolution on IMF conditions appears even more pronounced in the present study. Also, the time delay between IMF changes and effects on arcs can be determined more accurately.

The ionospheric flow measurements are provided by the SuperDARN radar network [*Greenwald et al.,* 1995; *Chisham et al.,* 2007]. This network consists of an array of high-latitude high-frequency radars, which provides flow measurements of the high-latitude ionosphere in both hemispheres. Data from a single radar provide only the line-of-sight velocity component. A global two-dimensional map of the ionospheric flows can be obtained using the so-called map potential method [*Ruohoniemi and Baker*, 1998]. This technique combines data from all available radars, supplemented by data from a statistical model to constrain the solution in regions where there is no data, to determine the distribution of the ionospheric electrostatic potential as an expansion of spherical harmonics. In the present study we use data that have been processed by the map potential method and show ionospheric velocity vectors that combine the line-of-sight component of the ionospheric flow observed by the radars with a perpendicular component that is derived from the global electrostatic potential fit (for details, see *Ruohoniemi and Baker* [1998]).

1.4. Polar Arc Classification

For the polar arc study in *Kullen et al.* [2002], image sheets containing plots every 4–6 min were produced for the entire time period of the statistical study (1 December 1998 to 28 February 1999). A fixed color scale was used, extending from 0.2 to 20 photons/(cm^2 s) to enhance even weakest auroral features with luminosity values close to the instrument threshold. As Polar was in the Northern Hemisphere at that time, the entire study is based on winter events where polar arcs are much more visible. During the winter season dayglow has an only limited effect on the visibility of the global auroral pattern. Sunlight appears either completely sunward of the auroral oval or dilutes only the dayside part of the oval.

The present study is based on the list of large-scale polar arcs from *Kullen et al.* [2002]. They identified 92 large-scale polar arcs in Polar UVI, which clearly separate from the main auroral oval and last for at least 10 min. Those 18 of the 92 large-scale polar arcs, where the evolution is unclear due to an insufficient field of view or extremely weak emissions over large periods of the arc lifetime, were excluded from the *Kullen et al.* [2002] data set, reducing the number of studied events to 74 large-scale polar arcs. The present work is based on these 74 large-scale polar arc events.

In addition to large-scale polar arcs there exist 146 polar arcs that have a lifetime of less than 10 min, are very short and/or are not clearly separated from the oval. These were in *Kullen et al.* [2002] referred to as "small splits." Furthermore, during one third of all large-scale polar arc events, secondary arcs appear in the polar cap. The large majority of these secondary arcs are very small or faint such that most of these could be categorized as small splits as well. In the present study neither small splits nor secondary arcs are included in the data analysis.

In a second step, the 74 large-scale polar arcs were sorted into different subgroups by *Kullen et al.* [2002], solely based on their spatial evolution. The majority of the 74 events consist of polar arcs that separate from the dawn or dusk oval side and move at least slightly into the polar cap such that a clear separation from the oval is seen (i.e., oval and arc are separated by a region on the image that is dominated by the image background color). These were classified by *Kullen et al.* [2002] as oval-aligned or moving arcs depending on how much they propagate during their lifetime. Oval-aligned arcs were defined in *Kullen et al.* [2002] as those polar arcs that are clearly separated from the dawn or dusk oval side but did not show considerable motion during their existence (28 arcs). A further 11 arcs that experienced a considerable motion over the polar cap along the dawn-dusk meridian during their lifetime have been referred to as moving arcs. Seven of these arcs move (nearly) over the entire polar cap. The four remaining moving arcs reach very high latitudes (87–90° along the dawn-dusk meridian) but do not pass the noon-midnight meridian

There exist 22 events that have been classified in *Kullen et al.* [2002] as "bending arcs." As already discussed in the introduction, bending arcs deviate strongly from both oval-aligned and moving arcs by bending into the polar cap rather than moving in the dawn-duskward direction. In Figure 1 five examples of such bending arcs are shown. These examples have been selected for a more detailed study as dayside SuperDARN data are available around arc formation, and Polar UVI provides a near-global view on these. A sixth event for which these criteria are fulfilled is not shown here, as it is analyzed and discussed in detail in *Carter et al.* [2015]. Each row in Figure 1 shows the temporal evolution of one bending arc. All plots consist of LBHL Polar UV images with a 36 s integration time. For each bending arc event a different color scale is used to enhance the arcs as much as possible in the plots. For all five events, the first plot shows the oval before an arc has developed (first column), in the next plot (second column) traces of a bending arc formation can be identified. The third plot shows the first image where a bending arc has clearly formed (defined as arc start time in the statistics). The arc intersection with the oval at that point of time is marked as a white cross. The MLT location of the cross is used in the following analysis as arc start location.

The examples in Figure 1 show the typical characteristics of bending arcs: they are often extremely faint (close to the luminosity threshold of UVI) and last for some tens of minutes only. In half of the bending arc cases an (often small) arc appears approximately during the same time on the opposite oval side. For example, in Figure 1, such arcs can be identified for the duskside bending arc event in row 3 (tailward end of dawn arc visible during entire event), the dawnside bending arc event in row 4 (small duskside arc in last two plots), and the duskside bending arc event in row 5 (clear oval-aligned arc at dawn).

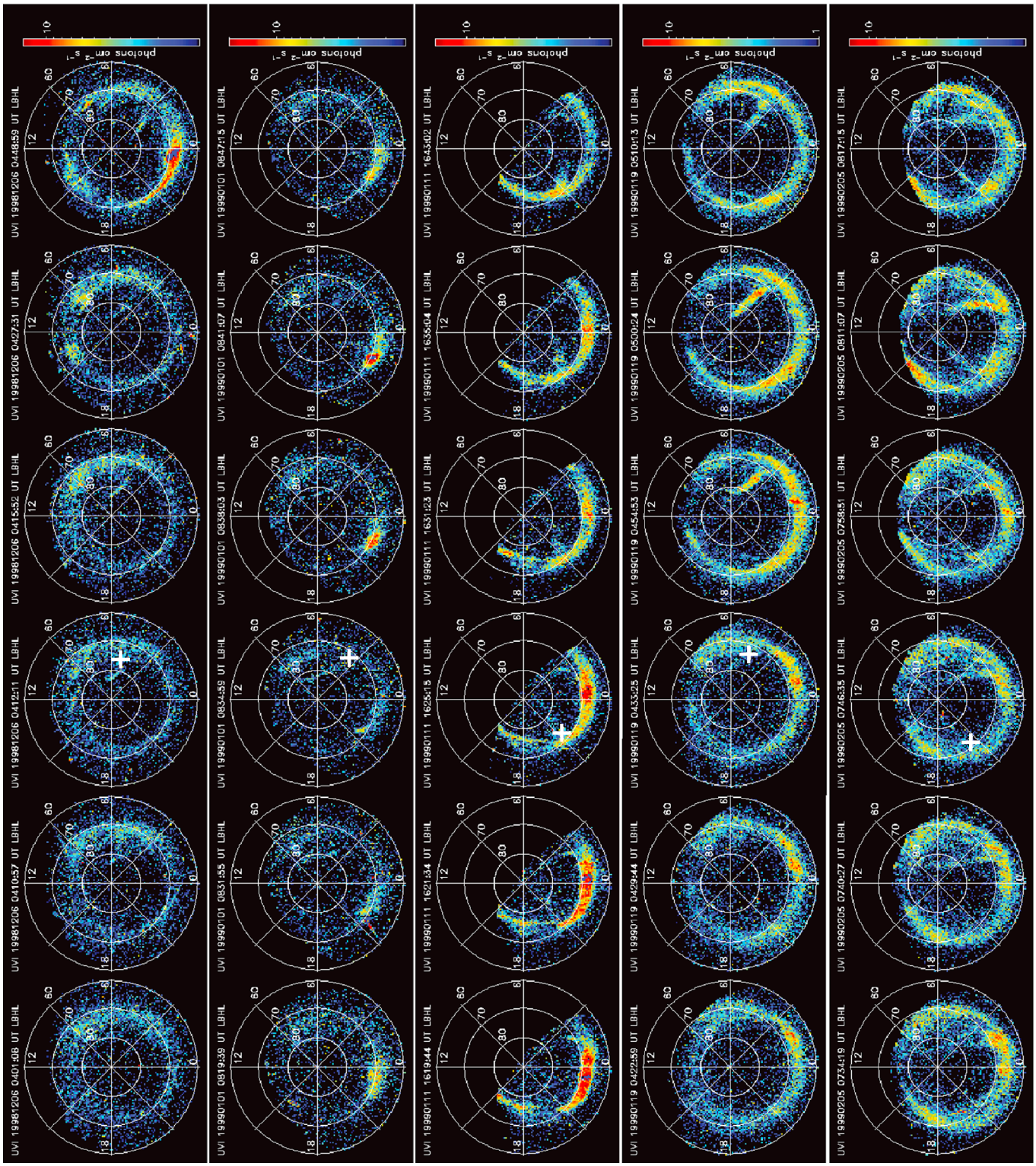

Figure 1. Temporal evolution of five bending arcs, as seen in LBH long images of Polar UVI. Each row corresponds to one event. The time of arc formation is shown in the third plot for each event. The arc intersection with the nightside oval at arc formation is marked with a white cross in that plot.

In the remaining 13 cases of *Kullen et al.*'s [2002] large-scale polar arc list, an arc develops at the nightside oval and seems to grow into the empty polar cap. In the cases where only one arc forms (6 events), the event is referred to as a nightside originating arc (referred to by *Kullen et al.* [2002] as midnight arcs). Nearly all of these single, nightside originating arcs evolve from a bright, thick bulge along the nightside poleward boundary of a thick and active oval during the late recovery phase of a substorm. In a few cases (7 events), three or more arcs occur simultaneously, referred to as multiple arc events. For these events, at least one arc forms close to midnight, while at least one arc separate from the dawn or dusk oval side.

To get as accurate information about the different arc types as possible, the cases described by *Kullen et al.* [2002] as "hybrid events" are removed in the present study when showing results for each of the five individual polar arc groups (oval-aligned, bending, moving, nightside-originating, or multiple arcs). For hybrid events a categorization is difficult as it is not clear to which group they should belong: seven polar arcs are so faint that they can only be detected when they appear in the middle of the polar cap; thus, according to the above described criteria they were categorized as oval-aligned arcs (no considerable motion) although there is a high probability that they are in fact moving or maybe even nightside originating arcs. Four moving arcs and one nightside originating arc appear so close to the oval that they may also have been categorized as oval-aligned arcs. Five bending arcs become clearly hook-shaped after formation, but have an otherwise very untypical evolution: four of these have an evolution similar to nightside originating arcs, but form on the dawn or dusk oval side, and one resembles an oval-aligned arc around the time of formation. Four of the five hybrid bending arcs appear during ongoing substorms with a thick and active recovery type oval. After removing the hybrid cases, the group of oval-aligned arcs is reduced to 21 events, bending arcs to 17, moving arcs to 7 and nightside originating arcs to 5 events only. The number of multiple arc events remains the same (7 events). Note that the results do not deviate much whether the hybrid cases are included or not, but the studied correlations are always slightly better when removing the hybrid cases from the five individual polar arc groups.

In the present study, the main focus is on bending arcs and in which way they differ from other polar arc types Thus, in several figures we divide the polar arcs into only two groups: bending arcs and all other polar arcs. The latter are from here on referred to as "regular polar arcs." The group of regular polar arcs consists of all 57 large-scale polar arcs that are not clear bending arcs. It includes hybrid events, as even these are clear large-scale polar arcs despite the fact that a categorization into one of the polar arc subgroups cannot be unambiguously be done.

As mentioned above, only the main arc during each polar arc event is examined. In the cases where secondary arcs occur simultaneously, they are excluded from further analysis (i.e., they are not included in the list of the 74 clear polar arcs). To be consistent, this concerns even those five (of 11) secondary arcs during bending arc events that are in fact clearly large-scale (see, e.g., the dawnside oval-aligned arc during the bending arc event in Figure 1, last row). Also, of each multiple arc event, only the main (most prominent) arc is examined further.

All 17 unambiguous bending arcs (i.e., excluding hybrid bending arc events) that are examined in detail in this study are listed in Table 1. The table includes date and time of formation (as well as time of disappearance) and the location of the nightside arc intersection with the oval at formation (and at disappearance).

1.5. Identification of Arc Start Time and Location

To estimate the polar arc start times as accurately as possible, all arc start times have been redetermined by visual inspection of all existing LBHL images, rather than by inspecting plots at 4–6 min cadence as done by *Kullen et al.* [2002]. The same color scale as in *Kullen et al.* [2002] and a dayglow removal algorithm are used to enhance even weakest auroral features in the UV images. For an as accurate as possible determination of the arc location, an algorithm is used to reduce the effect of a wobble that appears in one spacecraft direction of Polar. The wobble sometimes increases the effective pixel size from 50×50 km up to 50×250 km.

The first image, on which the arc is clearly separated from the oval (i.e., oval and arc are separated by an area with background color), is taken as arc start time. The arc location is here defined as the intersection of the nightside arc end with the poleward edge of the oval by drawing a line along the poleward oval boundary that crosses through the arc end. During many polar arc events, even parts of the oval are close to the UVI luminosity threshold (see, e.g., the bending arc event shown in Figure 1, row 2), such that the estimation

Table 1. Bending Arcs: Date, Time, and Location (in MLT and CGlat) of Nightside Arc Intersection With Oval at Arc Formation (Start Time) and Disappearance (End Time)

Date	Start Time	MLT at Start Time	CGLat at Start Time	End Time	MLT at End Time	CGLat at End Time
02-12-1998	03:59 UT	05.2	74.0	04:30 UT	04.0	74.0
05-12-1998	03:39 UT	05.3	72.0	04:28 UT	04.1	73.5
06-12-1998	04:12 UT	05.1	76.0	04:56 UT	02.6	71.0
16-12-1998	06:49 UT	18.3	74.0	07:04 UT	18.3	74.0
18-12-1998	03:18 UT	20.7	76.0	03:48 UT	19.0	81.0
01-10-1999	08:35 UT	03.5	72.0	08:47 UT	03.5	72.0
08-01-1999	11:48 UT	03.5	73.0	12:25 UT	02.5	70.5
11-01-1999	16:25 UT	21.3	72.5	16:48 UT	22.8	72.0
16-01-1999	00:51 UT	04.6	69.0	01:22 UT	03.5	72.0
19-01-1999	04:33 UT	04.5	73.0	05:15 UT	03.5	69.0
29-01-1999	13:54 UT	03.2	75.0	14:17 UT	01.6	73.0
30-01-1999	03:43 UT	04.5	72.0	03:48 UT	04.7	73.0
30-01-1999	04:42 UT	04.2	77.0	06:55 UT	03.0	78.0
05-02-1999	07:47 UT	20.6	71.5	08:54 UT	21.5	70.5
10-02-1999	15:33 UT	20.4	72.5	15:59 UT	21.5	73.0
14-02-1999	01:00 UT	01.9	69.0	01:19 UT	02.5	70.0
17-02-1999	02:24 UT	02.8	77.0	02:36 UT	02.8	73.0

of the magnetic latitude may be subject to an error of up to ±2° (see, e.g., the poleward oval boundary in Figure 1, row 1). As in the present study only the MLT position of the arc is investigated further; possible errors in estimating the magnetic latitude do not affect the results. The determination of MLT is accurate enough for our purpose, due to a clearly identifiable MLT location of the arc. We estimate the error in determining the MLT position as ±0.1 MLT, for a few extreme cases as ±0.2 MLT. Usually, the center of the arc at its oval intersection is taken as MLT location. In cases with strong luminosity differences within the arc, the brightest point along the arc intersection with the oval (which is in most cases nearly identical with the center of the arc) is taken as arc location instead.

2. Results and Discussion

2.1. Characteristics of Bending Arcs

A visual reinspection of all available Polar UV images around arc formation shows that for those bending arc events with good Polar UV coverage of the dayside oval (8 of 17 events), the dayside tip of the arc separates from the dayside oval at formation. In the remaining nine cases, the UV images do not cover the dayside part of the oval at arc formation (four cases) or the spacecraft is too close to the horizon (three cases) such that no information about the dayside tip of the bending arc can be gained. As can be seen from the bending arc examples shown in Figure 1, obviously, the spatial resolution and luminosity threshold of Polar UVI are nearly not good enough for a detailed analysis of arc formation of the very faint bending arcs. Images with a better resolution and/or particle data would be necessary to get more accurate information about where exactly the tip of the arc splits off the oval. However, it can be estimated that in those cases where the tip of the arc can be discerned on the image (e.g., rows 1, 2, and 4 in Figure 1) it appears 2–3 MLT away from noon before the arc starts to bend into the polar cap. For the bending arc in row 5, images close to the arc start time (that are not shown here) indicate that even in that case the tip of the arc is originally attached to noon. In row 3, the dayside part of the oval is out of field of view from Polar UVI. How long time after formation the tip of a bending arc remains attached to the dayside part of the oval, cannot be determined with certainty from the UV images. It is clear, though, that at the end of the arc lifetime (sixth column) only the nightside part of the arc is attached to the oval.

The observation that the tip of bending arcs splits off the dayside oval is in fact a defining feature of that arc type; although this was not included in the original definition by *Kullen et al.* [2002] who defined bending arcs as "hook-shaped poleward-moving arcs where the sunward end of the arc separates from the main oval and moves toward the other side of the oval whereas the antisunward end remains fixed." Also (as will be shown further down), this definition is not entirely correct as the nightside end of a bending arc does not always stay fixed but moves in most cases slightly tailward during the arc lifetime. As the original definition is not precise enough to identify unambiguously bending arcs, we define bending arcs here more precisely as polar arcs with one end (the dayside tip) separating from the prenoon or postnoon dayside oval before moving

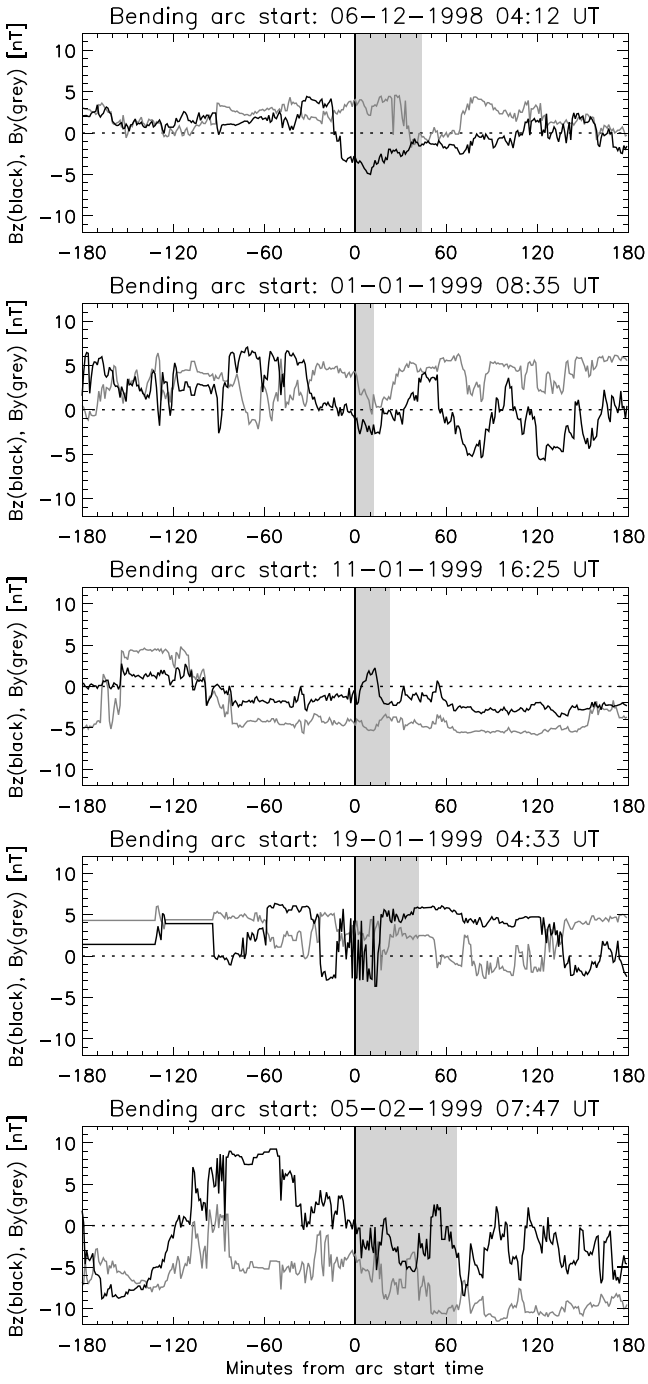

Figure 2. IMF B_z (black) and IMF B_y (gray) using OMNI solar wind data for the five bending arcs shown in Figure 1.The gray shaded area marks the arc lifetime of each bending arc event. Date and time in the title refer to the point of time at which the arc starts to form.

poleward and antisunward into the polar cap, while the nightside end of the arc remains attached to the oval such that the arc becomes hook-shaped after a while.

The IMF conditions during which the five bending arcs of Figure 1 are formed are shown in Figure 2 using OMNI data. IMF B_z (black) and IMF B_y (gray) are shown up to 3 h before and after arc formation. The arc lifetime is marked as a gray shaded area. A comparison of location (Figure 1) and IMF B_y sign at arc formation (Figure 2) shows that bending arcs form on the dawn side during positive B_y and on the dusk oval side during negative IMF B_y, as previously reported in *Kullen et al.* [2002].

Figure 2 illustrates nicely typical IMF conditions for bending arcs. In four of the five events there appears an IMF turn to southward IMF within 20 min around arc formation. At arc formation, IMF B_y dominates over B_z. In all but one event, IMF B_z was predominantly northward the last 2 h before the arc appears. Such IMF behavior is common for bending arcs. Of those 16 bending arcs with existing IMF data (a) IMF B_z was predominantly northward the last 2 h before arc formation in 75% of the cases, (b) for 82% a turn toward southward IMF appears ±30 min around bending arc start time and for 75% a turn toward northward IMF within ±30 min around the arc end time, and (c) in 69% of the cases $|B_y| \gg |B_z|$ at arc formation. For one bending arc (29 January 1999), no data exists ±1 h around arc formation. These trends can be seen even more clearly in Figure 3.

2.2. IMF Conditions and Arc Location of Bending and Regular Polar Arcs

In Figure 3 the average IMF conditions around bending (red curves) and regular polar arcs (black curves) are shown for IMF B_z (Figure 3, left) and the IMF clock angle (Figure 3, right). The plots contain the results of superposed epoch analysis plots centered on the start time of each arc. The left and right plots show the mean values of IMF B_z and IMF clock angle up to 3 h before and after arc start (vertical line) for both groups of polar arcs. To be able to examine the ratio between IMF B_y and B_z, the IMF clock angle is here defined as the angle between the absolute value of IMF B_y and IMF B_z. The dotted curves give the 2-sigma deviation from the mean values.

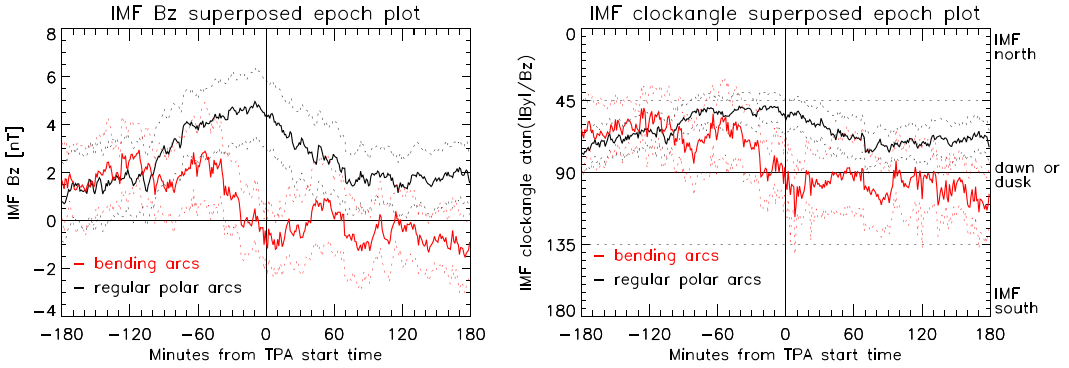

Figure 3. Superposed epoch curves of IMF B_z (left plot) and IMF clock angle (atan($|B_y|/B_z$)) (right plot) up to 3 h before and after each arc starts to form (plain vertical line) using OMNI solar wind data. The red superposed epoch curve results from all clear bending arcs, the black curve from regular polar arcs (i.e., all arcs except bending arcs). The dotted curves give the 2-sigma deviation from the mean values.

The plots in Figure 3 confirm what is known from many previous studies: regular polar arcs appear typically during hours of predominantly northward IMF. Looking at the IMF B_z plot in more detail shows that about 100 min before the arc starts to form, average IMF B_z rises to untypically high magnitudes, reaching 4–5 nT during the last hour, which is clearly higher than the typical magnitude of 3.0 nT for northward IMF (taking the mean value of IMF B_z during all time periods with northward IMF of the three months long survey). The mean IMF clock angle of regular polar arcs decreases from nearly 80° 3 h before to about 50° 1.3 h before arc formation. This means, during the last 1.3 h before arc formation the magnitude of IMF B_z is on average nearly equal to IMF B_y. Thus, it is highly probable that high-latitude lobe reconnection during nonzero IMF B_y conditions dominates the hours around arc formation. High-latitude lobe reconnection appears in all polar arc models focusing on the tail deformation for nonzero and/or an IMF B_y sign reversal during northward IMF and its topological connection to polar arcs as, e.g., in *Slinker et al.* [2001], *Kullen and Janhunen* [2004], *Naehr and Toffoletto* [2004], and *Tanaka et al.* [2004]. Such IMF clock angles are also consistent with the suppression of Dungey cycle convection, as required in the tail reconnection polar arc model outlined by *Milan et al.* [2005].

Bending arcs appear during IMF conditions that differ considerably from those of regular polar arcs. After hours of (on average) weakly northward IMF, the IMF becomes purely dawn or duskward with B_z values near zero about 20 min before arc formation (IMF clock angle around 90°). An IMF turn to weakly southward IMF appears on average 10 min before the arc starts to form. The IMF remains on average southward (but still B_y-dominated) for about 35 min, which also corresponds to the average lifetime of bending arcs. This means, B_y-dominated dayside reconnection is expected to start on average about 20 min before bending arc formation. Note that as the arc start time is defined as the point of time, where the arc becomes for the first time clearly visible on Polar UVI (which has a limited resolution), it may be possible that the arc started to form several minutes earlier (see also Figure 1, column 2, indicating in some cases a 5–10 min earlier arc formation). Thus, it may be that bending arcs form at the same time as dayside reconnection starts.

In Figure 4, the location of the nightside intersection of the arc with the poleward oval boundary is shown at the time of arc formation for all 74 clear polar arc events. The figure contains two plots with a polar view of the northern hemisphere in CGlat-MLT coordinates. Figure 4 (left) shows the location of the nightside arc location at the time of arc formation (the start time). Figure 4 (right) shows both the location at the start time (indicated by a cross) and at the end time (opposite end of straight line starting with a cross). To identify the different arc types, the 17 clear bending arcs are marked in red, the 7 clear moving arcs in blue, and all other regular polar arcs (50 events) in black.

In Figure 4 (left) a clear difference between bending and regular polar arcs is seen. All (except two) bending arcs start to form within narrow dawnside (2.8–5.3 MLT) and duskside sectors (20.4–21.3 MLT) sunward of most regular arcs: 82% of all bending arcs appear sunward of 21 and 3 MLT, whereas 81% of all regular polar arcs appear tailward of those local times along the nightside oval. The largest spread in both latitude and longitude of arc locations occurs for moving arcs.

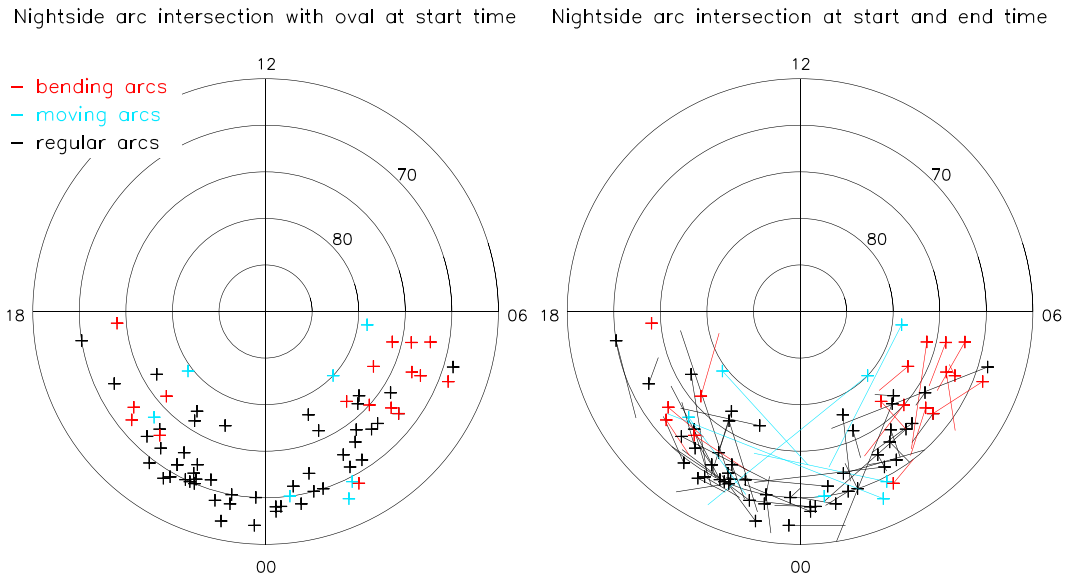

Figure 4. Location of all polar arcs at arc start time and end time shown in a polar plot of the northern hemisphere in MLT-CGLat coordinates: The arc location is defined as the intersection of the nightside end of the polar arc with the poleward oval boundary. The left plot shows the arc location at the point of time where the polar arc starts to form; the right plot shows the arc location at start time (cross) and end time of all polar arcs (end of straight line connected to cross). The red, blue and black crosses correspond to arc locations of bending, moving and all remaining regular arcs, respectively.

As can be seen from Figure 4 (right), the location of the arc's nightside intersection with the oval changes over the lifetime of most polar arcs. Bending arcs experience only a small tailward motion of the nightside arc end during their lifetime (on average 1.01 MLT). Regular polar arcs show a large spread in MLT between start and end time. As expected from the definition of moving arcs, the largest displacement between arc start and end point is found for these. For 5 of the 7 moving arcs, the nightside arc end moves to the opposite oval side.

The results in Figure 4 (right) also illustrate why the group of moving arcs in *Kullen et al.* [2002] is not identical with moving arcs as defined in *Fear and Milan*'s [2012a] study. *Fear and Milan* [2012a] used a less restrictive definition, requiring a motion of the arcs tailward end of over 2 MLT in either direction (i.e., even arcs are included which move away from the noon-midnight meridian), whereas *Kullen et al.* [2002] required a considerable motion over the polar cap toward the noon-midnight meridian (when looking at the arc motion along the dawn-dusk meridian), resulting even in a much larger displacement of the nightside arc location for most events. Figure 4 shows 18% of all polar arcs that have not been identified as moving arcs in *Kullen et al.* [2002] move more than 2 MLT during their lifetime, while two of the *Kullen et al.* [2002] moving arcs move less than 2 MLT along the oval (although even in these two cases the arc moves—according to the definition of moving arcs in *Kullen et al.* [2002]—far poleward when looking at the arc motion along the dawn-dusk meridian). This means, care has to be taken when comparing the results of those two studies, as the moving arcs of *Kullen et al.* [2002] are nearly entirely a subgroup of *Fear and Milan*'s [2012a] moving arcs.

2.3. Dependence of Arc Location on IMF B_y

Previous studies have shown that the local time at which polar arcs are observed depends upon the IMF B_y component. Here this correlation is reinvestigated with help of *Kullen et al.*'s [2002] polar arc data set. In Figure 5, the same analysis regarding IMF B_y dependence of the initial polar arc location is performed as in *Fear and Milan* [2012a]. They used the Spearman's rank instead of the Pearson's correlation. It assesses how well the relationship between two variables can be described using a monotonic (but not necessary linear) function. For a direct comparison, we use the same correlation coefficient here.

Figure 5 shows the Spearman's rank coefficient of the correlation between the initial MLT location of the nightside arc intersection with the oval and hourly averaged IMF B_y up to 50 h before and after arc formation. The black curve shows the correlation for all regular polar arcs (i.e., excluding the 17 clear bending arcs but including all hybrid events) of *Kullen et al.*'s [2002] polar arc data set. For comparison, the *Fear and Milan* [2012a] results are overplotted in red.

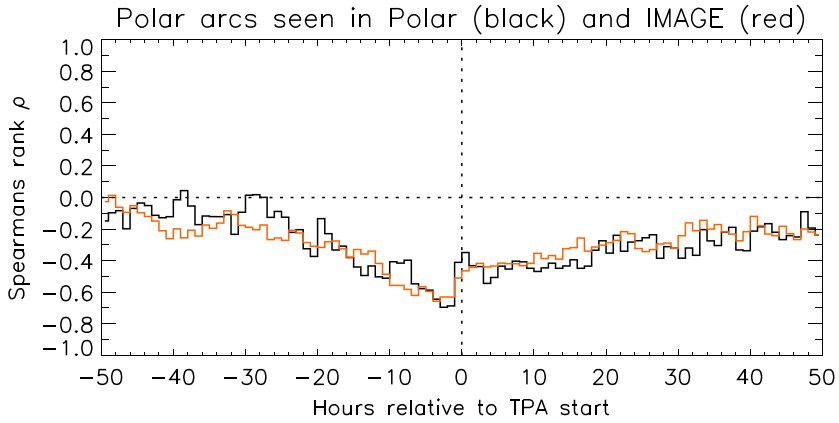

Figure 5. The Spearman's rank correlation between IMF B_y and the MLT locations of the nightside intersections of the polar arcs with the oval at arc formation (=start time) for hourly averaged IMF B_y values up to ±50 h from time point of arc formation. The red curve shows the results for *Fear and Milan*'s [2012b] polar arc data set based on IMAGE data; the black curve shows the results for all regular polar arcs (excluding clear bending arcs) identified in Polar UVI by *Kullen et al.* [2002] (present study).

The main trend, known from many previous studies [e.g., *Gussenhoven*, 1982], that duskside arcs appear typically during duskward IMF and dawnside arcs during dawnward IMF conditions is expressed in the negative correlation between IMF B_y and initial arc location. The results for *Kullen et al.*'s [2002] and *Fear and Milan*'s [2012a] data sets are astonishingly similar despite the fact that different auroral imagers have been used and different time periods have been studied: for the present data set, Polar UVI images from winter 1998/1999 have been used, *Fear and Milan*'s [2012a] polar arc data set is based on IMAGE data from 2000 to 2005. Due to the higher number of events in *Fear and Milan*'s [2012a] polar arc data set (131 as compared to 57 regular polar arcs in the present study), the red curve is slightly smoother than the black curve. Both curves closely overlap over large parts of the 100 h time period around arc formation. The main trend in the red curve is the same as for the black curve: a very high correlation between IMF B_y and initial location of polar arcs is found for several hours before arc formation until ~1 h before the arc appears, at which point the correlation drops from around 0.7 to 0.4. The correlation remains at that lower level for many hours after arc formation.

In Figure 6 the dependence of polar arc location on IMF B_y is shown in more detail by using 20 min IMF B_y averages and splitting up the polar arcs into the five different polar arc subgroups as defined in *Kullen et al.* [2002]. For comparison, IMF B_y superposed epoch analysis plots are shown in the right column for each arc type. As the sign of IMF B_y controls which side of the oval polar arcs form, the sign of IMF B_y is reversed for those arcs that form on the dusk oval side in the superposed epoch analysis plots. The results are shown for (from top to bottom): all regular polar arcs (i.e., excluding only the 17 bending arcs), oval-aligned arcs, moving arcs, nightside originating arcs, main arc of multiple arc events, and bending arcs.

When using 20 min IMF B_y averages (Figure 6, top left) the best Spearman's rank correlation for regular polar arcs is found for B_y conditions 100–120 min before arc formation, instead of 2–3 h (*Kullen et al.*'s [2002] data set) or 3–4 h (*Fear and Milan*'s [2012a] data set) for hourly averaged IMF B_y values, shown in Figure 5. Although the precise peak of the Spearman's rank correlation shifts depending on data set and time period over which IMF B_y is averaged over, there is a common trend in all three plots: A stronger correlation is obtained for any hour chosen between 1 and 7 h before the arc formed than in the hour immediately before formation. Considering that the formation of polar arcs is according to several polar arc models tightly connected to IMF B_y induced changes in the magnetotail, the 1–2 h time delay between IMF B_y and its effect on initial arc location is in agreement with a recent report by *Rong et al.* [2015] of a 60–90 min time delay until IMF B_y penetrates the inner magnetotail. The small differences in the results of Figure 5 and 6 (top left) indicate the case-to-case variation in the time taken for the IMF B_y component to influence the initial arc location. Also, as the remaining plots in the left column of Figure 6 show, the optimal time delay depends strongly on the polar arc type.

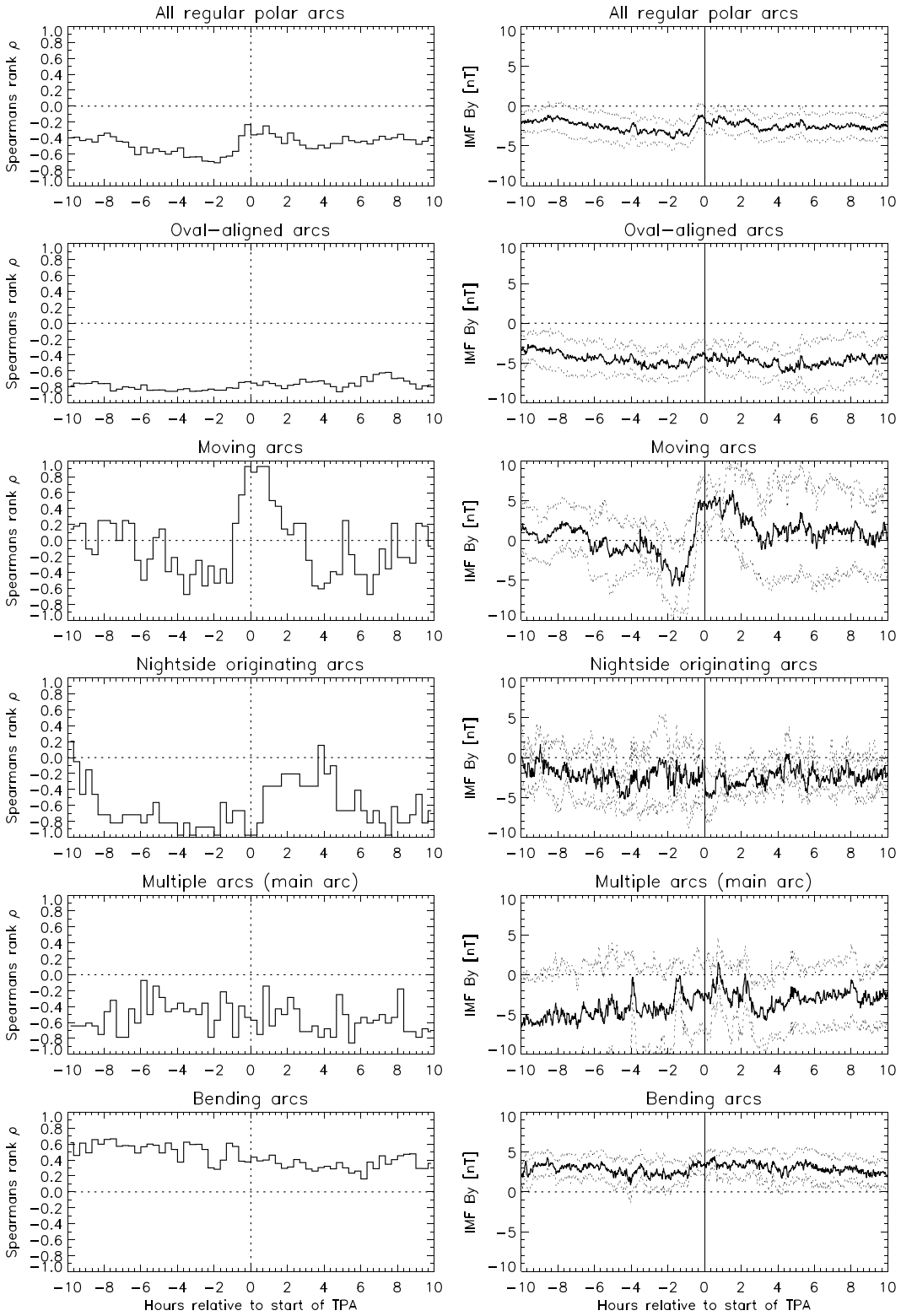

Figure 6. IMF B_y dependence of different polar arc types. Left column: Spearman's rank correlation between IMF B_y and the MLT location of the nightside polar arc end at arc formation for 20 min averaged IMF B_y values up to ±10 h from arc start time. Right column: Superposed epoch analysis plot of IMF B_y, centered at arc start time. The sign of IMF B_y is reversed for all arcs that form on the dusk oval side. The plots show (from top to bottom) all regular polar arcs except bending arcs, oval-aligned arcs, moving arcs, nightside originating arcs, main arc of each multiple arc event, and bending arcs.

For oval-aligned arcs, the correlation stays at very high negative values around −0.8 during the entire 20 h time period around arc formation. Also, for the groups of nightside originating and multiple arc events the correlation is negative many hours around arc formation. For moving arcs the correlation changes 1 h before arc formation from negative (−0.5) to positive values (+0.9). Only for bending arcs the correlation is positive during the entire 20 h time period. Note, the maximum correlation for bending arcs (0.6) is lower than for all other arc types.

Studying the time evolution of mean IMF B_y for the different arc types (Figure 6, right column) helps to understand better the B_y-MLT correlation plots for the different polar arc types. Taking into account that in the superposed epoch analysis plots, the sign of IMF B_y has been switched for duskside polar arcs, the plots for the different polar arc types show for dawnside (duskside) oval-aligned arcs average IMF B_y is negative (positive) and stays on average nearly constant for the 20 h time period around arc formation, whereas dawnside (duskside) moving arcs appear on average some tens of minutes after an IMF B_y sign change from negative to positive (positive to negative). The results for nightside originating and multiple arcs are less clear (partly due to the small number of events, see also the high 2-sigma spread) but the tendency is the same as for oval-aligned arcs. Bending arcs occur on the opposite oval side as regular polar arcs: dawnside (duskside) bending arcs form during IMF conditions with on average hours of constantly positive (negative) B_y values.

By comparing the plots in the left and right columns of Figure 6, it becomes clear why the (negative) correlation between IMF B_y and location of oval-aligned arcs does not exhibit a clear dependence on the time span between B_y and arc formation: the average IMF B_y component remains at nearly constant (negative) values the hours around arc formation (the same holds approximately for nightside originating and main arc of multiple arcs). That polar arcs with little subsequent motion form during periods of steady IMF has already been pointed out by *Kullen et al.* [2002] and *Fear and Milan* [2012a]; however, this connection is seen even more clearly in the present plots.

The IMF B_y superposed epoch analysis plot for moving arcs reveals that an IMF B_y sign change takes place on average about 40 min before a moving arc forms. This is reflected in the switch from negative to positive Spearman's rank correlations 1 h before arc formation. This in turn is consistent with the fact that the moving arcs in *Kullen et al.* [2002] are defined as those which show a considerable motion over the polar cap toward (and often across) the noon-midnight meridian, resulting in a selection of events which nearly all move across to the other side of the polar cap. As shown in several previous observational studies [e.g., *Cumnock et al.,* 2002] and MHD simulations [*Slinker et al.,* 2001; *Kullen and Janhunen*, 2004; *Naehr and Toffoletto*, 2004; *Tanaka et al.,* 2004], such conditions require a change in the sign of the IMF B_y component, whereas if a smaller motion or even a motion in the opposite direction is included (i.e., away from the noon-midnight meridian), as was considered in the case of *Fear and Milan*'s [2012a] moving arcs, then the net result is a drop in the correlation from a negative correlation beforehand to zero correlation at the time of arc formation. As already discussed by *Fear and Milan* [2012a], the different definition of moving arcs is also the reason why their study produced similar results for nonmoving but slightly different results for moving arcs as compared to the study by *Kullen et al.* [2002].

Figure 7 consists of MLT- B_y scatterplots for three polar arc types. The plots show the MLT location at arc formation for oval-aligned (left), moving (middle), and bending (right) arcs versus 20 min averaged IMF B_y. In the top row the results are shown for the average IMF B_y component during the last 20 min before arc formation. The bottom row shows plots for average IMF B_y between 100 and 120 min before arc formation. The Pearson's correlation coefficient (r), the Spearman's rank correlation coefficient (ρ), and the linear regression line are plotted into the scatterplots.

As expected from Figure 6, the correlation for oval-aligned arcs is stronger if calculated with 20 min averaged IMF B_y values 2 h before than at arc formation. As shown by *Fear and Milan* [2012a], the MLT location depends not only on the sign of IMF B_y but also on its magnitude. For moving arcs, the correlation is much weaker 2 h before arc formation than for oval-aligned arcs. This is due to the strongly different time scales of an IMF B_y sign change from case to case. The effect of the IMF B_y sign reversal is reflected in opposite signs of B_y at arc formation as compared to 2 h earlier in all but one case (in that case only a large B_y magnitude decrease appears). Most interesting are the results for bending arcs. From the scatterplots it becomes clear that the

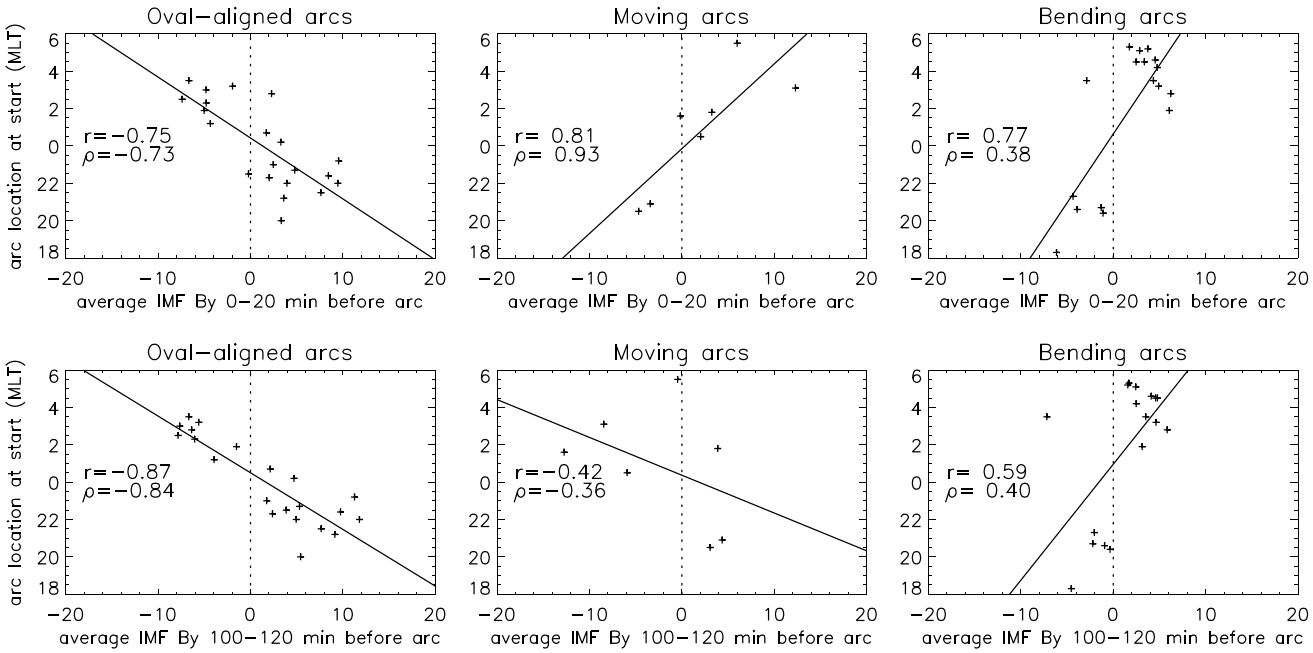

Figure 7. Scatterplots for polar arc location (in MLT) versus IMF B_y values for (left) oval-aligned arcs, (middle) moving arcs, and (right) bending arcs. The arc location is defined as the intersection of the nightside end of the polar arc with the poleward oval boundary at the point of time where a polar arc starts to form. In the top row, IMF B_y is averaged the last 20 min before arc start, in the bottom row, IMF B_y is averaged over a 20 min time period 100-120 min before arc start.

arc location has a clear dependence on IMF B_y sign, but not on its magnitude. They appear on the dusk side of the oval for dawnward IMF and on the dawnside for duskward IMF, but the nightside arc intersection with the oval appears for all events several hours MLT away from midnight. This explains the not very high values of the Spearman's rank correlation for bending arcs in Figure 6. Note that there is one apparent exception (at 3.8 MLT) where average IMF B_y is negative although the arc appears at dawn, which appears to contradict the above trend. This is the only bending arc event (8 January 1999), where IMF B_y is strongly varying around arc formation. *Carter et al.* [2015], whose study is based on that event, show that B_y points to the expected direction when using IMF data from the WIND spacecraft (which was closer to Earth than ACE, on which OMNI data are based in that case) thus even in that case the bending arc appears most probably for the expected sign of IMF B_y.

2.4. Ionospheric Plasma Flows During Arc Formation

Figure 8 summarizes the auroral and ionospheric observations for those six bending arcs for which Polar UVI covers (at least part of) the dayside oval and SuperDARN scatter was present at the poleward oval boundary in that region. One other event (8 January 1999) for which there was good coverage in Polar UVI SuperDARN is omitted from Figure 8, as this event is discussed in detail in *Carter et al.* [2015]. We refer to their paper for that case. IMF conditions and the spatial evolution of all arcs in Figure 8, except case (e) are shown in Figures 1 and 2. Case (e) is not included in Figures 1 and 2 due to a too small UVI field of view and lack of IMF data around arc formation. However, the Polar UV image boundary is close enough to the region covered by SuperDARN data to be able to study the flows in that event as well by interpolation of the oval boundary from the dayside edge of the Polar UVI field of view.

In Figure 8 each panel is plotted on MLT-CGlat grid, with noon MLT at the top, midnight at the bottom, and dawn and dusk at the right and left, respectively. The panels show northern hemisphere SuperDARN plasma flow vectors determined from map potential analysis [*Ruohoniemi and Baker,* 1998], and averaged over a 10 min period. Each plasma flow plot is superimposed on a Polar UVI image in gray scale where the nightside oval intersection at arc formation is shown by a red dot. The time of the UV image and the start time of the 10 min averaged vector plots are written above each panel. Most of the panels correspond to the 10 min period containing the arc's initial emergence, but in Figure 8a a later time has been chosen to better highlight

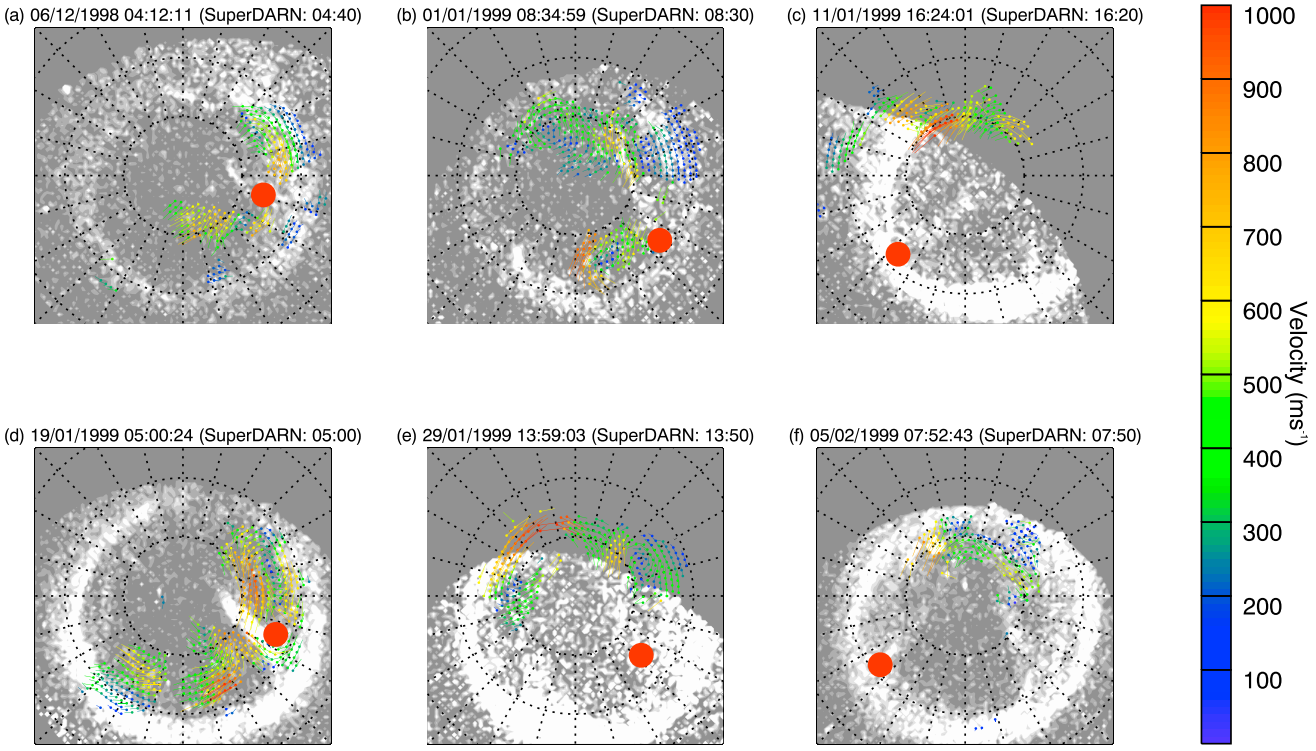

Figure 8. SuperDARN plasma flow vectors overlaid over Polar UVI for all bending arcs with good Polar UVI and SuperDARN coverage of the dayside oval close to arc formation. The flow vectors are averaged over a 10 min time period, the start time of the chosen period is indicated in each panel. SuperDARN flow vectors are presented such that the origin of each vector is marked by a dot; the direction of the flow at that point is indicated by the direction of the line, and the magnitude of the flow speed is indicated by both the length of the line and color of the vectors.

the observed dayside ionospheric flows. As can be seen from Table 1, the bending arc of Figure 8a still exists during the time for which the plasma flow plot is shown.

In each event shown in Figure 8, antisunward plasma flows are observed across the poleward edge of the dayside auroral oval at some dayside local time sunward of the arc's nightside intersection with the oval (indicated by the red dot). As the poleward oval boundary can be taken as an estimate of the open/closed field line boundary, flows across the dayside oval into the polar cap can be interpreted as a signature of ongoing dayside reconnection.

Therefore, for the events shown in Figures 8b–8f (for which the ionospheric flows plotted correspond to the 10 min period containing the initial formation of the arc), the flows indicate that dayside reconnection was occurring as the arc formed. The same holds for the bending arc event (8 January 1999) discussed in *Carter et al.* [2015]. For the event in Figure 8a, similar flows to those plotted were observed at the time at which the arc formed, but the flow across the oval boundary was not as clear as at the times plotted. However, the presence of clear reconnection signatures shortly after the bending arc first appeared strongly suggests that even this arc formed during dayside reconnection.

Overall, the plasma flow observations for the seven SuperDARN conjunction events with flows across the dayside open-closed field line boundary in each event combined with the results from the IMF analysis in Figure 3, showing a rotation of the IMF clock angle from northward to weakly southward around arc formation, are strong evidence that bending arcs appear during recently started dayside reconnection. Figure 2 proves that this holds for each individual event presented in Figure 8: around arc formation IMF B_z is weakly southward (cases a,b, and c) or close to zero (cases d and f). IMF B_y dominates over B_z in all cases. These are typical conditions during which B_y-dominated dayside reconnection is expected to occur.

Evidence that bending arcs may form as a direct result of dayside reconnection has been provided in *Carter et al.* [2015]. DMSP particle data indicate a magnetosheath or cusp origin of the bending arc that is examined

in their paper. This means that the arc most probably appears on recently opened field lines. As PMAFs are known to form on newly opened field lines that are caused by pulsed dayside reconnection (FTE events) [*Milan et al.*, 2000, and references therein], *Carter et al.* [2015] proposed that bending arcs may be created by a similar formation mechanism despite some apparent differences in occurrence frequency, lifetime, and shape of the auroral features.

Appearing as isolated events with an average lifetime of 30 min, bending arcs are (in opposite to PMAFs) most probably not quasiperiodic features. PMAFs are known to split off the dayside oval and often appear in a sequence with events separated on average every ~8 min. They occur as a direct result of pulsed reconnection (FTEs) and move within a few minutes into the polar cap before they disappear [e.g., *Fasel,* 1995, and references therein]. Also, *Carter et al.* [2015] pointed out that the bending arc examined in their paper must be the auroral signature of a single flux transfer event. Whether the isolated occurrence of bending arcs is real, or (as would be expected for auroral features caused by a sequence of FTEs) is followed by a series of further arcs with a luminosity or spatial extent that is below the Polar UVI threshold (as is suggested in *Carter et al.* [2015]), remains to be shown. It is clear, though, that bending arcs occur not as frequently as FTEs, which exist during half the time when IMF is southward [*Russell et al.,* 1996]. While PMAFs may occur during any southward (sometimes even northward) IMF condition [*Fasel*, 1995] in connection with FTEs, bending arcs form typically only after prolonged periods of northward IMF, during near zero or weakly negative IMF B_z conditions, as is shown in Figure 3.

The length of bending arcs and PMAFs are (at least for some events) comparable. As can be seen by studying PMAFs with global imagers instead of all-sky cameras, even PMAFs may have a length of several MLT and a nightside oval intersection far from noon [*Milan et al.,* 2000]. The hook-shaped form of bending arcs, on the other hand, has not been reported for PMAFs. Based on the observation that the speed at which the tip of a bending arc propagates poleward is similar to the surrounding plasma flow velocity, *Carter et al.* [2015] suggested that the plasma pushes the arc in a poleward and antisunward direction, which eventually causes the arc to bend into the polar cap. The similarity between the plasma flow pattern of the cases shown in Figure 8 with *Carter et al.'s* [2015] bending arc event strongly suggests that this is the case for all bending arcs.

Figure 9 summarizes the auroral and ionospheric observations for the 10 regular polar arcs (i.e., excluding bending arcs) identified by *Kullen et al.* [2002] for which there was ionospheric scatter coincident with the nightside auroral oval between midnight MLT and the initial MLT location of the arc's intersection with the nightside oval. The figure adopts a similar format to Figures 2, 4, and 5 of *Fear and Milan* [2012b]. Each event is summarized by three panels (one row), and identified by a letter a to j. Underneath the label is a two letter code identifying the "type" of arc as identified by *Kullen et al.* [2002]: "oa" indicates an oval-aligned arc; "mu" (multiple) indicates the main arc of a multiple arc event, and "mn" (midnight) indicates a nightside originating arc. Figure 9 (middle column) shows the nightside part of the oval at the time of the arc formation. The initial arc location has been indicated by a red dot, which is also plotted in the other panels. To help orient the reader, Figure 9 (left column) shows the Polar UVI observation a short while later, once the arc has formed more fully. Figure 9 (right column) shows the SuperDARN velocity vectors calculated from map potential analysis from a selected time in the 30–40 min preceding the start of the arc—hence, the three plots for each event are ordered going backward in time from left to right. Figure 9 (right column) is constructed following the same procedure as *Fear and Milan* [2012b] (i.e., 10 min blocks of SuperDARN data were combined to produce map potential vectors representing flows averaged over this time scale). The vectors are superimposed on a concurrent auroral image.

In the events shown in Figures 9a–9g, there are clear east/west flows observed that are coincident with the auroral oval. For the cases shown in Figures 9b, 9d, 9f, and 9g, these take the form of TRINNI events; the eastward or westward end of the flow channel coincides with the location at which the arc subsequently appears (indicated by the red dot) which is consistent with the predictions made by *Milan et al.* [2005]. In Figures 9c and 9e, the nightside flows are less asymmetric, but these correspond to two events which formed near midnight MLT. The only exception in this subgroup is the event in row (a), where the arc forms at postmidnight (at about 3 MLT), but the division between eastward and westward returning flows is closer to 1 MLT. However, the left-most image in Figure 9a shows an arc observed closer to 2 MLT; it is not clear whether this is the same feature as identified in the middle panel, and it is possible that the flows

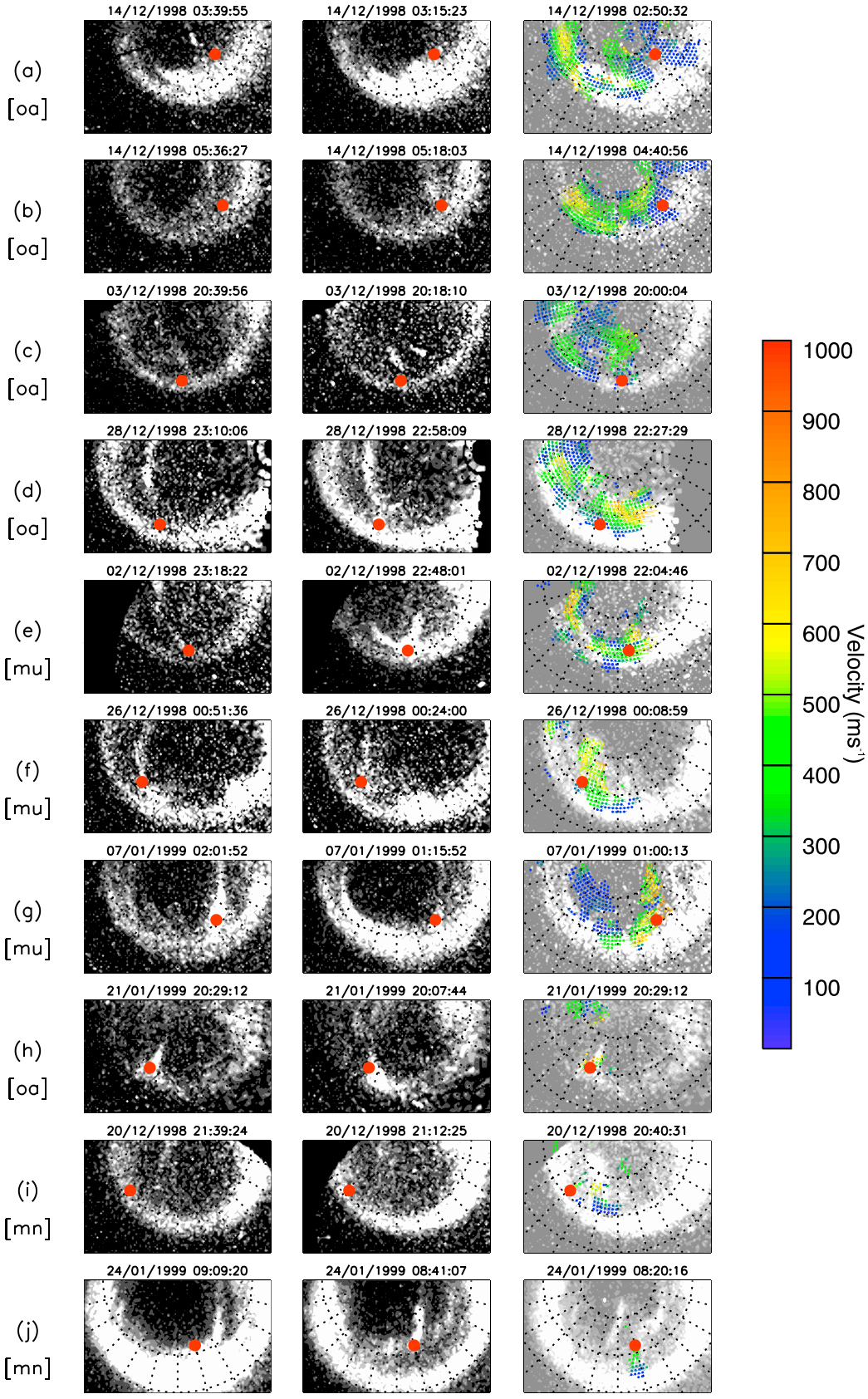
14/12/1998 03:39:55
14/12/1998 03:15:23
14/12/1998 02:50:32
(a)
[oa]
14/12/1998 05:36:27
14/12/1998 05:18:03
14/12/1998 04:40:56
(b)
[oa]
03/12/1998 20:39:56
03/12/1998 20:18:10
03/12/1998 20:00:04
(c)
[oa]
28/12/1998 23:10:06
28/12/1998 22:58:09
28/12/1998 22:27:29
(d)
[oa]
02/12/1998 23:18:22
02/12/1998 22:48:01
02/12/1998 22:04:46
(e)
[mu]
26/12/1998 00:51:36
26/12/1998 00:24:00
26/12/1998 00:08:59
(f)
[mu]
07/01/1999 02:01:52
07/01/1999 01:15:52
07/01/1999 01:00:13
(g)
[mu]
21/01/1999 20:29:12
21/01/1999 20:07:44
21/01/1999 20:29:12
(h)
[oa]
20/12/1998 21:39:24
20/12/1998 21:12:25
20/12/1998 20:40:31
(i)
[mn]
24/01/1999 09:09:20
24/01/1999 08:41:07
24/01/1999 08:20:16
(j)
[mn]
1000
900
800
700
600
500
400
300
200
100
Velocity (ms⁻¹)

Figure 9

observed at 02:50 UT (right column) are associated with this (possibly separate) event. Figures 9h–9j shows three further events for which there was not much scatter on the nightside auroral oval, but where there is a localized patch of scatter indicating antisunward flows onto the nightside oval in the same MLT as the arc was subsequently seen to form. Such flows are highly suggestive of localized closure of magnetotail flux in this location.

To summarize the results of Figure 9, in (at least) 9 of the 10 events, there is evidence for nightside plasma flows starting at the initial arc location, at least four of which are clear TRINNI events. This confirms the predictions by *Milan et al.* [2005] that polar arcs form at the division between east and westward flows. As TRINNIs are caused by magnetotail reconnection [e.g., *Grocott et al.,* 2005], these events indicate that changes in the magnetotail topology caused by tail reconnection may play a vital role in the formation of polar arcs, as proposed by *Milan et al.* [2005]. Also, the results of Figure 9 confirm the statistical observations by *Fear and Milan* [2012b]. It is interesting to note that the consistent flows in Figure 9 span all types of regular polar arcs identified by *Kullen et al.* [2002] (apart from moving arcs, for which there were no events with sufficient scatter), which is strongly suggestive of a common formation mechanism for all regular polar arcs.

We also examined the SuperDARN data for evidence of nightside reconnection flows (TRINNIs) during the 17 bending arc events, but found no evidence for such signatures. Conclusions on this point are limited by the fact that there was often a lack of ionospheric scatter coincident with the nightside oval. However the absence of any clear signatures of strong plasma flows along the nightside oval in contrast to the events plotted in Figure 9 and in the results of *Fear and Milan* [2012b] is consistent with our overall conclusion (and that of *Carter et al.* [2015]) that the "bending arcs" identified by *Kullen et al.* [2002] are in fact signatures of dayside, rather than nightside, reconnection.

3. Summary and Conclusions

The polar arc data set by *Kullen et al.* [2002] has been reinvestigated regarding IMF dependence, polar arc location, and ionospheric plasma flows during arc formation. In the present study, more accurate IMF data (OMNI data), and a more exact determination of arc start time and location (Polar UVI) are used. An analysis of SuperDARN data is performed for those events where coincident ionospheric scatter exists. The data set consists of 74 clear large-scale polar arcs, identified in Polar UV images of the Northern Hemisphere during three winter months in 1998/1999, 17 of which are so-called bending arcs. The remaining arcs of the data set are referred to as regular polar arcs (most of these are elsewhere called transpolar).

A more detailed visual analysis of existing Polar UV images than in *Kullen et al.* [2002] allowed a more precise definition of bending arcs: a polar arc is referred to as bending arc if it forms on the dawn- or duskside oval with the dayside tip of the arc splitting off the oval in the prenoon or postnoon sector before moving poleward and antisunward into the polar cap while its nightside end remains attached to the oval, such that the arc becomes hook-shaped after a while.

To be able to compare the results of two independent polar arc data sets, the investigation of the initial arc location, its IMF dependence and connection with ionospheric plasma flows has been done in a similar way as in the statistical studies by *Fear and Milan* [2012a, 2012b]. Overall, the results of the present study confirm the observations reported in *Fear and Milan* [2012a, 2012b] for regular polar arcs but not for bending arcs.

The outcome of the present investigation combined with the results from *Kullen et al.* [2002] shows that bending arcs are distinctly different from regular polar arcs. Bending arcs are much fainter, have a shorter lifetime, and appear on the opposite oval side from and farther sunward than most regular polar arcs (81% bending arcs appear sunward; 81% regular arcs appear tailward of 21 and 3 MLT). Dependent on the sign

Figure 9. SuperDARN flow vectors overlaid over Polar UVI for all regular polar arcs with good SuperDARN coverage on the nightside oval at arc formation. The figure has the same format as Figure 8. The panels are ordered in the same way as Figures 2, 4, and 5 of *Fear and Milan* [2012a]: Each event is summarized in one row with Polar UV images 20 min (left column) after arc formation at (middle column) arc formation and 40 min (right column) before arc formation). SuperDARN ionospheric flow vector plots from a selected time in the 30–40 min preceding the start of the arc are overlaid on UVI plots of the right column.

of IMF B_y, bending arcs form on the dawn (duskward IMF) or dusk oval side (dawnward IMF). The analysis of IMF and SuperDARN data shows, contrary to regular arcs, that bending arcs are highly probable to appear in connection with recently started dayside reconnection: ionospheric plasma flows from the dayside oval into the polar cap and the typically weakly southward IMF conditions during arc formation are strongly indicative for ongoing reconnection along the dayside magnetopause. The observed antisunward plasma flows appear (depending on the sign of IMF B_y) in the prenoon or postnoon polar cap just sunward of the arc pushing it in antisunward direction which probably causes its hook-shaped form, as first suggested in the single case study by *Carter et al.* [2015]. Based on observations that a bending arc appears on recently opened field lines during conditions favorable for dayside reconnection, *Carter et al.* [2015] proposed that bending arcs are signatures of flux transfer events in a similar way as poleward moving auroral forms. The results of the present study are consistent with the formation mechanism, described in *Carter et al.* [2015] which suggests that their explanation is valid for bending arcs in general.

The examination of plasma flows along the nightside oval during the formation of polar arcs shows that 9 of the 10 examined regular polar arcs form close to the location where dawnward and duskward plasma flows separate, independent on the polar arc type. At least four of these appear during TRINNI events indicating that tail reconnection is involved in the formation of the arcs. The results are in agreement with the statistical results of *Fear and Milan* [2012b] and confirm the validity of *Milan et al.*'s [2005] predictions for all arc types except bending arcs. For bending arcs no evidence of nightside reconnection flows was found which suggests that these are probably not connected to tail reconnection processes.

Summarizing the results of the present study, *Kullen et al.* [2002] and *Fear and Milan* [2012a] about the influence of IMF B_y on polar arc location, the following scenario appears: the sign of IMF B_y determines on which oval side polar arcs occur. Regular polar arcs in the Northern Hemisphere appear typically close to the dawn (dusk) oval side for dawnward (duskward) IMF B_y. Once formed, the only arcs which move considerably are those where B_y has significantly changed magnitude or even sign. The initial arc location is influenced by IMF B_y conditions that appeared at least 1-2 h earlier. In the present study, the best correlation between initial arc location and IMF B_y is found for a 100–120 min time delay.

Acknowledgments

We would like to acknowledge the support from ISSI, Bern, for participation in the ISSI International Team on Polar Cap Auroras, during which the present study was initiated and discussed. The authors thank George Parks and the Polar UVI team for providing UV images. OMNI solar wind data were obtained from the CDA Web. We are grateful for access to SuperDARN data through University of Leicester. A.K. was partially supported by the Swedish National Space Board. S.E.M. and J.A.C. were supported by the Science and Technology Facilities Council (UK), grant ST/K001000/1. R.C.F. was supported by STFC Ernest Rutherford Fellowship ST/K004298/1.

References

Carter, J. A., S. E. Milan, R. C. Fear, A. Kullen, and M. R. Hairston (2015), Dayside reconnection under IMF B_y-dominated conditions: The formation and movement of bending arcs, *J. Geophys. Res. Space Physics*, *120*, 2967–2978, doi:10.1002/2014JA020809.

Chang, S. W., et al. (1998), A comparison of a model for the theta aurora with observations from Polar, wind, and SuperDARN, *J. Geophys. Res.*, *103*, 17,367–17,390, doi:10.1029/97JA02255.

Chisham, G., et al. (2007), A decade of the Super Dual Auroral Radar Network (SuperDARN): Scientific achievements, new techniques and future directions, *Surv. Geophys.*, *28*(1), 33–109, doi:10.1007/s10712-007-9017-8.

Cowley, S. (1981), Magnetospheric asymmetries associated with the y-component of the IMF, *Planet. Space Sci.*, *29*(1), 79–96, doi:10.1016/0032-0633(81)90141-0.

Craven, J. D., L. A. Frank, C. T. Russell, E. J. Smith, and R. P. Lepping (1986), The global auroral responses to magnetospheric compressions by shocks in the solar wind: Two case studies, in *Solar Wind–Magnetosphere Coupling*, edited by Y. Kamide and J. A. Slavin, pp. 367–380, Terra Sci., Tokyo.

Craven, J. D., J. S. Murphree, L. A. Frank, and L. L. Cogger (1991), Simultaneous optical observations of transpolar arcs in the 2 polar caps, *Geophys. Res. Lett.*, *18*, 2297–2300, doi:10.1029/91GL02308.

Cumnock, J. (2005), High-latitude aurora during steady northward interplanetary magnetic field and changing IMF B_y, *J. Geophys. Res.*, *110*, A02304, doi:10.1029/2004JA010867.

Cumnock, J., J. Sharber, R. Heelis, M. Hairston, and J. Craven (1997), Evolution of the global aurora during positive IMF B_z and varying IMF B_y conditions, *J. Geophys. Res.*, *102*, 17,489–17,497, doi:10.1029/97JA01182.

Cumnock, J., J. Sharber, R. Heelis, L. Blomberg, G. Germany, J. Spann, and W. Coley (2002), Interplanetary magnetic field control of theta aurora development, *J. Geophys. Res.*, *107*(A7), 1108, doi:10.1029/2001JA009126.

Elphinstone, R. D., K. Jankowska, J. S. Murphree, and L. L. Cogger (1990), The configuration of the auroral distribution for interplanetary magnetic field-Bz northward 1. IMF B_x and B_y dependencies as observed by the Viking satellite, *J. Geophys. Res.*, *95*, 5791–5804, doi:10.1029/JA095iA05p05791.

Fairfield, D. H. (1979), Average configuration of the geomagnetic tail, *J. Geophys. Res.*, *84*, 1950–1958, doi:10.1029/JA084iA05p01950.

Fasel, G. (1995), Dayside poleward moving auroral forms: A statistical study, *J. Geophys. Res.*, *100*, 11,891–11,906.

Fear, R., and S. Milan (2012a), The IMF dependence of the local time of transpolar arcs: Implications for formation mechanism, *J. Geophys. Res.*, *117*, A03213, doi:10.1029/2011JA017209.

Fear, R., and S. Milan (2012b), Ionospheric flows relating to transpolar arc formation, *J. Geophys. Res.*, *117*, A09230, doi:10.1029/2012JA017830.

Fear, R., S. Milan, R. Maggiolo, A. Fazakerley, I. Dandouras, and S. Mende (2014), Direct observation of closed magnetic flux trapped in the high-latitude magnetosphere, *Science*, *346*(6216), 1506–1510, doi:10.1126/science.1257377.

Frank, L. A., J. D. Craven, J. L. Burch, and J. D. Winningham (1982), Polar views of the Earths aurora with Dynamics Explorer, *Geophys. Res. Lett.*, *9*, 1001–1004, doi:10.1029/GL009i009p01001.

Frank, L. A., et al. (1986), The theta-aurora, *J. Geophys. Res.*, *91*, 3177–3224, doi:10.1029/JA091iA03p03177.
Goudarzi, A., M. Lester, S. Milan, and H. Frey (2008), Multi-instrumentation observations of a transpolar arc in the northern hemisphere, *Ann. Geophys.*, *26*(1), 201–210.
Greenwald, R., et al. (1995), DARN/SUPERDARN - a global view of the dynamics of high-latitude convection, *Space Sci. Rev.*, *71*(1–4), 761–796, doi:10.1007/BF00751350.
Grocott, A., S. Cowley, and J. Sigwarth (2003), Ionospheric flow during extended intervals of northward but B_y-dominated IMF, *Ann. Geophys.*, *21*(2), 509–538.
Grocott, A., S. Badman, S. Cowley, T. Yeoman, and P. Cripps (2004), The influence of IMF B_y on the nature of the nightside high-latitude ionospheric flow during intervals of positive IMF B_z, *Ann. Geophys.*, *22*(5), 1755–1764.
Grocott, A., T. Yeoman, S. Milan, and S. Cowley (2005), Interhemispheric observations of the ionospheric signature of tail reconnection during IMF-northward non-substorm intervals, *Ann. Geophys.*, *23*(5), 1763–1770.
Grocott, A., T. Yeoman, S. Milan, O. Amm, H. Frey, L. Juusola, R. Nakamura, C. Owen, H. Reme, and T. Takada (2007), Multi-scale observations of magnetotail flux transport during IMF-northward non-substorm intervals, *Ann. Geophys.*, *25*(7), 1709–1720.
Gusev, M. G., and O. A. Troshichev (1986), Hook-shaped arcs in dayside polar-cap and their relation to the IMF, *Planet. Space Sci.*, *34*(6), 489–496, doi:10.1016/0032-0633(86)90087-5.
Gussenhoven, M. S. (1982), Extremely high-latitude auroras, *J. Geophys. Res.*, *87*, 2401–2412, doi:10.1029/JA087iA04p02401.
Huang, C. Y., J. D. Craven, and L. A. Frank (1989), Simultaneous observations of a theta-aurora and associated magnetotail plasmas, *J. Geophys. Res.*, *94*, 10,137–10,143, doi:10.1029/JA094iA08p10137.
Ismail, S., and C. I. Meng (1982), A classification of polar-cap auroral arcs, *Planet. Space Sci.*, *30*(4), 319–330, doi:10.1016/0032-0633(82)90037-X.
Kaymaz, Z., G. L. Siscoe, J. G. Luhmann, R. P. Lepping, and C. T. Russell (1994), Interplanetary magnetic-field control of magnetotail magnetic-field geometry - IMP-8 observations, *J. Geophys. Res.*, *99*, 11,113–11,126, doi:10.1029/94JA00300.
King, J., and N. Papitashvili (2005), Solar wind spatial scales in and comparisons of hourly Wind and ACE plasma and magnetic field data, *J. Geophys. Res.*, *110*, A02104, doi:10.1029/2004JA010649.
Kullen, A. (2000), The connection between transpolar arcs and magnetotail rotation, *Geophys. Res. Lett.*, *27*, 73–76, doi:10.1029/1999GL010675.
Kullen, A. (2012), Transpolar arcs: Summary and recent results, in *Auroral Phenomenology and Magnetospheric Processes: Earth and Other Planets, Geophys. Monogr. Ser.*, vol. 197, edited by A. Keiling et al., pp. 69–80, AGU, Washington, D. C., doi:10.1029/2011GM001183.
Kullen, A., and P. Janhunen (2004), Relation of polar auroral arcs to magnetotail twisting and IMF rotation: A systematic MHD simulation study, *Ann. Geophys.*, *22*(3), 951–970.
Kullen, A., M. Brittnacher, J. Cumnock, and L. Blomberg (2002), Solar wind dependence of the occurrence and motion of polar auroral arcs: A statistical study, *J. Geophys. Res.*, *107*(A11), 1362, doi:10.1029/2002JA009245.
Kullen, A., J. Cumnock, and T. Karlsson (2008), Seasonal dependence and solar wind control of transpolar arc luminosity, *J. Geophys. Res.*, *113*, A08316, doi:10.1029/2008JA013086.
Makita, K., C. I. Meng, and S. I. Akasofu (1991), Transpolar auroras, their particle-precipitation, and IMF-B_y component, *J. Geophys. Res.*, *96*, 14,085–14,095, doi:10.1029/90JA02323.
McEwen, D., and Y. Zhang (2000), A continuous view of the dawn-dusk polar cap, *Geophys. Res. Lett.*, *27*, 477–480, doi:10.1029/1999GL010761.
Meng, C. I. (1981), Polar-cap arcs and the plasma sheet, *Geophys. Res. Lett.*, *8*, 273–276, doi:10.1029/GL008i003p00273.
Meng, C. I., and S. I. Akasofu (1976), Relation between polar-cap auroral arc and auroral oval arc, *J. Geophys. Res.*, *81*, 4004–4006, doi:10.1029/JA081i022p04004.
Milan, S., M. Lester, S. Cowley, and M. Brittnacher (2000), Convection and auroral response to a southward turning of the IMF: Polar UVI, CUTLASS, and IMAGE signatures of transient magnetic flux transfer at the magnetopause, *J. Geophys. Res.*, *105*, 15,741–15,755, doi:10.1029/2000JA900022.
Milan, S., B. Hubert, and A. Grocott (2005), Formation and motion of a transpolar arc in response to dayside and nightside reconnection, *J. Geophys. Res.*, *110*, A01212, doi:10.1029/2004JA010835.
Murphree, J. S., and L. L. Cogger (1981), Observed connections between apparent polar-cap features and the instantaneous diffuse auroral oval, *Planet. Space Sci.*, *29*(11), 1143–1149, doi:10.1016/0032-0633(81)90120-3.
Naehr, S., and F. Toffoletto (2004), Quantitative modeling of the magnetic field configuration associated with the theta aurora, *J. Geophys. Res.*, *109*, A07202, doi:10.1029/2003JA010191.
Newell, P., and C. Meng (1995), Creation of theta-auroras: The isolation of plasma sheet fragments in the polar-cap, *Science*, *270*(5240), 1338–1341, doi:10.1126/science.270.5240.1338.
Newell, P., D. Xu, C. Meng, and M. Kivelson (1997), Dynamical polar cap: A unifying approach, *J. Geophys. Res.*, *102*, 127–139, doi:10.1029/96JA03045.
Newell, P., K. Liou, C. Meng, M. Brittnacher, and G. Parks (1999), Dynamics of double-theta aurora: Polar UVI study of January 10–11, 1997, *J. Geophys. Res.*, *104*, 95–104, doi:10.1029/1998JA900014.
Newell, P., K. Liou, and G. Wilson (2009), Polar cap particle precipitation and aurora: Review and commentary, *J. Atmos. Sol. Terr. Phys.*, *71*(2), 199–215, doi:10.1016/j.jastp.2008.11.004.
Owen, C. J., J. A. Slavin, I. G. Richardson, N. Murphy, and R. J. Hynds (1995), Average motion, structure and orientation of the distant magnetotail determined from remote-sensing of the edge of the plasma sheet boundary layer with E-greater-than-35 keV ions, *J. Geophys. Res.*, *100*, 185–204, doi:10.1029/94JA02417.
Peterson, W. K., and E. G. Shelley (1984), Origin of the plasma in a cross-polar cap auroral feature (theta-aurora), *J. Geophys. Res.*, *89*, 6729–6736, doi:10.1029/JA089iA08p06729.
Richmond, A. D. (1995), Ionospheric electrodynamics using magnetic apex coordinates, *J. Geomagn. Geoelectr.*, *47*(2), 191–212.
Rong, Z. J., A. T. Y. Lui, W. X. Wan, Y. Y. Yang, C. Shen, A. A. Petrukovich, Y. C. Zhang, T. L. Zhang, and Y. Wei (2015), Time delay of interplanetary magnetic field penetration into Earth's magnetotail, *J. Geophys. Res. Space Physics*, *120*, 3406–3414, doi:10.1002/2014JA020452.
Ruohoniemi, J., and K. Baker (1998), Large-scale imaging of high-latitude convection with Super Dual Auroral Radar Network HF radar observations, *J. Geophys. Res.*, *103*, 20,797–20,811, doi:10.1029/98JA01288.
Russell, C. T., G. Le, and H. Kuo (1996), The occurrence rate of flux transfer events, *Adv. Space Res.*, *18*, 8197.
Sandholt, P., and C. Farrugia (2007), Poleward moving auroral forms (PMAFs) revisited: Responses of aurorae, plasma convection and Birkeland currents in the pre- and postnoon sectors under positive and negative IMF B(y) conditions, *Ann. Geophys.*, *25*(7), 1629–1652.
Slinker, S., J. Fedder, D. McEwen, Y. Zhang, and J. Lyon (2001), Polar cap study during northward interplanetary magnetic field on 19 January 1998, *Phys. Plasmas*, *8*(4), 1119–1126, doi:10.1063/1.1355680.

Tanaka, T., T. Obara, and M. Kunitake (2004), Formation of the theta aurora by a transient convection during northward interplanetary magnetic field, *J. Geophys. Res.*, *109*, A09201, doi:10.1029/2003JA010271.

Torr, M. R., et al. (1995), A far-ultraviolet imager for the international solar-terrestrial physics mission, *Space Sci. Rev.*, *71*(1–4), 329–383, doi:10.1007/BF00751335.

Tsyganenko, N. A. (1989), A magnetospheric magnetic-field model with a warped tail current sheet, *Planet. Space Sci.*, *37*(1), 5–20, doi:10.1016/0032-0633(89)90066-4.

Tsyganenko, N. A., and D. Fairfield (2004), Global shape of the magnetotail current sheet as derived from Geotail and Polar data, *J. Geophys. Res.*, *109*, A03218, doi:10.1029/2003JA010062.

Tsyganenko, N. A., S. Karlsson, S. Kokubun, T. Yamamoto, A. Lazarus, K. Ogilvie, C. Russell, and J. Slavin (1998), Global configuration of the magnetotail current sheet as derived from Geotail, Wind, IMP 8 and ISEE 1/2 data, *J. Geophys. Res.*, *103*, 6827–6841, doi:10.1029/97JA03621.

Valladares, C. E., H. C. Carlson, and K. Fukui (1994), Interplanetary magnetic-field dependency of stable Sun-aligned polar-cap arcs, *J. Geophys. Res.*, *99*, 6247–6272, doi:10.1029/93JA03255.

Zhu, L., R. Schunk, and J. Sojka (1997), Polar cap arcs: A review, *J. Atmos. Sol. Terr. Phys.*, *59*(10), 1087–1126, doi:10.1016/S1364-6826(96)00113-7.